

HU-EP-06/12
BI-TP 2006/16
SFB/CPP-06-23

Overlap Hypercube Fermions in QCD

Simulations Near the Chiral Limit

Wolfgang Bietenholz^a and Stanislav Shcheredin^b

^a Institut für Physik
Humboldt Universität zu Berlin
Newtonstr. 15, D-12489 Berlin, Germany

^b Fakultät für Physik
Universität Bielefeld
D-33615 Bielefeld, Germany

The overlap hypercube fermion is a variant of a chirally symmetric lattice fermion, which is endowed with a higher level of locality than the standard overlap fermion. We apply this formulation in quenched QCD simulations with light quarks. In the p -regime we evaluate the masses of light pseudoscalar and vector mesons, as well as the pion decay constant and the renormalisation constant Z_A . In the ϵ -regime we present results for the leading Low Energy Constants of the chiral Lagrangian, Σ and F_π . To this end, we perform fits to predictions by chiral Random Matrix Theory and by different versions of quenched Chiral Perturbation Theory, referring to distinct correlation functions. These results, along with an evaluation of the topological susceptibility, are also compared to the outcome based on the standard overlap operator.

1 Overview

QCD at low energy cannot be handled by perturbation theory. Therefore it is often replaced by Chiral Perturbation Theory (χ PT) as an effective theory [1]. χ PT deals with fields for the light mesons (occasionally also nucleons) which are the relevant degrees of freedom in that regime. Here we present non-perturbative results for QCD itself — the fundamental theory — at low energy, and we also establish a connection to the most important parameters in χ PT. For such systems, chiral symmetry plays a central rôle, even though it is only realised approximately.

In general, it is notoriously problematic to regularise quantum field theories with massless (or light) fermions in a way, which keeps track of the (approximate) chiral symmetry. For instance, in the framework of dimensional regularisation this issue is analysed carefully in Ref. [2]. However, in the framework of the lattice regularisation there was substantial progress in this respect at the end of the last century (for a review, see Ref. [3]). At least for vector theories a satisfactory solution was found, which enables the simulation of QCD close to the chiral limit. But since this formulation is computationally demanding, production runs are limited to the quenched approximation up to now.

In this work, we present simulation results employing a specific type of chiral lattice fermions, denoted as the overlap hypercube fermion (overlap-HF). In Section 2 we briefly review its construction and discuss some properties, which are superior compared to the standard overlap formulation.

Section 3 is devoted to the regime, where the p -expansion of χ PT [4] is applicable (p -regime). Here we present simulation results for bare quark masses in the range from 16.1 MeV to 161 MeV. We measure the masses of light pseudoscalar and vector mesons, and the quark mass according to the PCAC relation. The latter fixes the axial-current renormalisation constant Z_A , which has a stable extrapolation to the chiral limit. We also present a matrix element evaluation of the pion decay constant F_π , where, however, such an extrapolation is less stable.

In a fixed volume $V \simeq (1.48 \text{ fm})^3 \times (2.96 \text{ fm})$, we further decrease the bare quark mass to $m_q \leq 8 \text{ MeV}$, which takes us into the ϵ -regime, i.e. the domain of the ϵ -expansion [5] in χ PT. The study of overlap-HFs in the ϵ -regime, and also the comparison to the standard overlap fermions under identical conditions, is the main issue of this work, which we present in Section 4. In that regime, finite size effects and the topological sectors play an extraordinary rôle.

Therefore, in Subsection 4.1 we first discuss the distribution of topological charges — defined by the fermion index — and the corresponding

susceptibility. Then we address the Low Energy Constants (LECs) of the chiral Lagrangian, which parametrise the finite size effects. Hence they can be extracted even from the ϵ -regime — i.e. from a relatively small volume — with their values in infinite volume, which are relevant in physics. In Subsection 4.2 we compare our results for the leading non-zero eigenvalue of the Dirac operator to the prediction by chiral Random Matrix Theory (RMT), which allows for a determination of the chiral condensate Σ .

Finally we return to F_π , which we evaluate in the ϵ -regime by means of two methods. In Subsection 4.3 we fit the correlation function of the axial-currents to a prediction by quenched χ PT, making use of the previously obtained values for Z_A and Σ . At last we work directly in the chiral limit (i.e. at zero quark mass) and consider the zero-mode contributions to the pseudoscalar correlation functions (Subsection 4.4). Again, a value for F_π emerges from a fit of our data to a prediction by quenched χ PT. However, the two versions of quenched χ PT that we apply to determine F_π differ by a subtlety in the counting rules for the quenched terms in the ϵ -expansion.

We summarise and discuss our results in Section 5. Part of them were included previously in a Ph.D. thesis [6] and in several proceeding contributions [7].

2 The overlap hypercube fermion in QCD

The lattice regularisation usually introduces a UV cutoff π/a , where a is the lattice spacing. However, a block variable Renormalisation Group Transformation (RGT) generates a lattice action on a coarser lattice — say, with a spacing $a' = 2a$ — which leaves the system unchanged, so that still the original cutoff matters [8]. Hence in this formulation the lattice artifacts are controlled by $2\pi/a'$, in contrast to the situation for a standard action. An infinite iteration of this blocking procedure leads in principle (for suitable RGT parameters) to a *perfect lattice action*, which is free of any cutoff artifacts.

In practice, for most systems perfect actions can only be constructed in some approximation, such as a classical RGT step [9, 10], and a truncation of the long-range couplings is needed. Exceptions are, for instance, the quantum rotor [11], the Gross-Neveu model at large N [12] and the free fermion, where explicitly parametrised perfect actions are known [13, 14]. Let us start from free Wilson-type fermions and iterate the

simple (blocking factor n) RGT

$$\begin{aligned}
e^{-S'[\bar{\psi}', \psi']} &= \int \mathcal{D}\bar{\psi} \mathcal{D}\psi \exp \left\{ -S[\bar{\psi}, \psi] - \frac{\mu}{a} \sum_{x'} \left[\bar{\psi}'_{x'} - \frac{1}{n^{(d+1)/2}} \sum_{x \in x'} \bar{\psi}_x \right] \right. \\
&\quad \left. \times \left[\psi'_{x'} - \frac{1}{n^{(d+1)/2}} \sum_{x \in x'} \psi_x \right] \right\}. \quad (2.1)
\end{aligned}$$

Here x (x') are the sites of the original, fine (blocked, coarse) lattice, populated by the spinor fields $\bar{\psi}$, ψ ($\bar{\psi}'$, ψ'), with the lattice action S (S'), and $x \in x'$ are the sites x in the n^d block with centre x' (in d dimensions, and $n = 2, 3 \dots$). $\mu \neq 0$ is a real, dimensionless RGT parameter. After an infinite number of iterations, a perfect, free lattice action $S^*[\bar{\psi}, \psi]$ emerges, with a Dirac operator D consisting of a vector term plus a scalar term,

$$S^*[\bar{\psi}, \psi] = a^d \sum_{x,y} \bar{\psi}_x D_{xy} \psi_y, \quad D_{xy} = \gamma_\mu \rho_\mu(x-y) + \lambda(x-y), \quad (2.2)$$

(where we denote the spacing on the final lattice again by a). For a finite RGT parameter μ , the scalar term λ is non-zero. Then this action is *local*, since the couplings in ρ_μ and λ decay exponentially at large distances $|x-y|$ even at zero fermion mass (x and y are lattice sites) [13]. This is satisfactory from the conceptual perspective, but in view of practical applications the couplings need to be truncated to a short range. A useful truncation scheme works as follows [15]: one first optimises the RGT so that the locality of the operator D is maximal, hence the truncation is minimally harmful. Then one constructs the perfect fermion action on a small, periodic lattice of size 3^4 (where we now specify $d = 4$). The couplings obtained in this way are finally used also in larger volumes. This is a truncation to a *hypercube fermion* (HF) operator D_{HF} with

$$\text{supp}[\rho_\mu(x-y)], \text{supp}[\lambda(x-y)] \subset \left\{ x, y \mid |x_\nu - y_\nu| \leq a, \forall \nu \right\}. \quad (2.3)$$

The free HF still has excellent scaling properties [15, 16].

At mass zero, the perfect fermions are *chiral*, since D solves the Ginsparg-Wilson relation (GWR) [17]

$$D\gamma_5 + \gamma_5 D = \frac{a}{\mu} D\gamma_5 D \quad (2.4)$$

for a simple RGT of the type (2.1), with a transformation parameter $\mu \approx 1$. The GWR is obvious for free perfect fermions, but it also persists under gauge interaction. Classically perfect Dirac operators solve the

GWR as well [18], and the free HF operator D_{HF} does so to very good approximation, as the spectrum shows [19].

In our HF formulation of lattice QCD [15, 20, 6]¹, the gauge field is treated rather ad hoc, since it is the fermionic part which is most delicate. Hence we use the standard Wilson gauge action, and the Dirac operator is gauged as follows: if the lattice spinors $\bar{\psi}_x$ and ψ_y are coupled by $D_{\text{HF},xy}$ — i.e. if they are located in the same lattice unit hypercube — we connect them by the shortest lattice paths and multiply the compact link variables on these paths. The normalised sum of these link products is denoted as a *hyperlink* between $\bar{\psi}_x$ and ψ_y (a fully explicit description is given in Refs. [20, 6]).

In addition, we replace the simple links in the above procedure by fat links, $U_\mu(x) \rightarrow (1 - \alpha)U_\mu(x) + \frac{\alpha}{6} \sum [\text{staples}]$, where α is a parameter to be optimised.

This HF is nearly rotation invariant, but its mass is subject to a significant additive renormalisation [15]. Criticality can be approximated again by amplifying all the link variables by a suitable factor $u > 1$. At last, in the vector term only they are also multiplied by an extra factor $v \lesssim 1$; this hardly alters the critical point, but it improves chirality, i.e. it moves D_{HF} closer to a GWR solution. The fat link, e.g. with α in the range 0.3...0.6, helps further in this respect [22, 6].

An optimisation of that kind was performed previously for quenched QCD at $\beta = 6$ [23]. Here we present the more difficult construction at $\beta = 5.85$, which corresponds to a lattice spacing of $a \simeq 0.123$ fm.² As a compromise between various optimisation criteria, we chose the following parameters [6]

$$u = 1.28, \quad v = 0.96, \quad \alpha = 0.52, \quad \mu = 1, \quad (2.5)$$

and the HF couplings are still those identified for the massless, truncated perfect, free fermion [15]. The physical part of the spectrum of this D_{HF} for a typical configuration at $\beta = 5.85$ is shown in Fig. 1. We also mark some of the eigenvalues with maximal real part; they reveal a striking difference from Wilson fermion spectra, which extend to much larger real parts. Moreover, we include the low eigenvalues for an alternative set of parameters, which moves the HF close to criticality. In that case we recognise a good approximation to the circle in the complex plane with centre and radius $\mu = 1$, which characterises an exact solution to the GWR (2.4). However, for the practical purposes in this paper, we prefer the parameters in eq. (2.5) (the advantages are a faster convergence and

¹For recent applications in thermodynamic systems, see Ref. [21].

²Throughout this work, we refer to the Sommer scale [24] for physical units. We do not keep track of possible errors in that scale.

a better locality if the HF operator is inserted in the overlap formula, which we are going to discuss next).

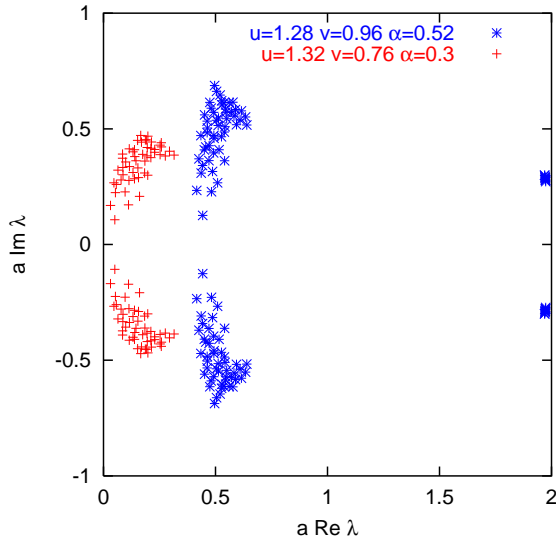


Figure 1: *The low lying part of the spectrum of D_{ovHF} , plus eigenvalues with maximal real part, for a typical configuration at $\beta = 5.85$ on a 8^4 lattice. We show one set of parameters which provides a good approximation to criticality and to the spectral Ginsparg-Wilson circle. However, for practical purposes we prefer the parameterisation (2.5), which leads to the other set of eigenvalues shown in this Figure.*

Of course, due to the truncation and the imperfect gauging, the scaling and chirality of this HF are somewhat distorted. At least chirality can be corrected again by inserting D_{HF} into the overlap formula [25]

$$D_{\text{ov}} = \frac{\mu}{a} \left(1 + A / \sqrt{A^\dagger A} \right), \quad A := D_0 - \frac{\mu}{a}. \quad (2.6)$$

This formula yields a solution to the GWR (2.4), provided that D_0 is a γ_5 -Hermitian lattice Dirac operator, $D_0^\dagger = \gamma_5 D_0 \gamma_5$. Another condition is that a value for μ must be available, which separates — for typical configurations at the gauge coupling under consideration — the (nearly) real part of the spectrum of D_0 in a sensible way into small (physical) eigenvalues and large eigenvalues (at the cutoff scale). Thus the physical eigenvalues are separated from the doublers, and we obtain the correct number of flavours. γ_5 -Hermiticity holds for example for the Wilson operator D_{W} and for D_{HF} , and for instance at $\beta = 6$ good values for μ can easily be found in both cases [26, 23].

$D_0 = D_{\text{W}}$ is the kernel of the *standard overlap operator* formulated by H. Neuberger [25]; we denote it by D_{N} . In this case, D_{W} changes drastically as it is inserted into the overlap formula (2.6). In contrast, D_{HF} is

already an approximate Ginsparg-Wilson operator, hence the transition to the corresponding overlap operator, $D_{\text{HF}} \rightarrow D_{\text{ovHF}}$, is only a modest modification,

$$D_{\text{ovHF}} \approx D_{\text{HF}} , \quad (2.7)$$

particularly in view of the eigenvalues with large real parts. In both cases, a lattice modified but exact chirality is guaranteed [27] through the GWR. The correct axial anomaly is reproduced in all topological sectors for the standard overlap fermion [28], as well as the overlap-HF [29]. But other important properties are strongly improved for D_{ovHF} compared to D_{N} , due to the construction of D_{HF} and relation (2.7).³

Let us first consider the condition number of the Hermitian operator $A^\dagger A$, i.e. the argument of the square root in the overlap formula (2.6). In our simulations, we project out the lowest 30 modes of $A^\dagger A$ — which are treated separately — and we approximate the remaining part by a Chebyshev polynomial to an absolute accuracy of 10^{-12} . The polynomial degree which is needed for a fixed precision is proportional to the square root of the condition number

$$c_{31} := \frac{\lambda_{\max}}{\lambda_{31}} , \quad \text{with } \lambda_{\max} \ (\lambda_{31}) : \text{ maximal (31}^{\text{st}}) \text{ eigenvalue of } A^\dagger A . \quad (2.8)$$

The values for $\langle c_{31} \rangle$, given in Table 1, show that the required polynomial degree for D_{ovHF} is a factor ≈ 5 lower. The computational effort is roughly proportional to this degree (the computation of the lowest modes of $A^\dagger A$ and their separate treatment are minor issues in terms of the computing time). On the other hand, the use of the HF kernel is computationally more expensive than D_{W} by about a factor 15, so that an overhead by a factor ≈ 3 remains. We hope for this factor to be more than compensated by the virtues of D_{ovHF} , in particular by an improved scaling due to the perfect action background of D_{HF} and relation (2.7). That property is very well confirmed for the free fermion [19] and for the 2-flavour Schwinger model (with quenched configurations, but measurement data re-weighted by the fermion determinant) [30]. But the corresponding scaling behaviour in QCD is not explored yet.

An important aspect that we do explore here is the locality. For this purpose, we put a unit source at the origin, $\eta_x = \delta_{x,0}$, and measure the expectation value of the function [26]

$$f_{\max}(r_1) := \max_y \left\{ \|D_{\text{ov},yx}(U)\eta_x\| \mid \|y\|_1 = r_1 \right\} . \quad (2.9)$$

³The concept of improving properties of D_{ov} beyond chirality by choosing a more favourable kernel than D_{W} was suggested in Ref. [19] and meanwhile implemented in several variants [30, 22, 31, 10, 32].

	β	D_N	D_{ovHF}
$\langle c_{11} \rangle$	5.85	4266(194)	179(10)
$\langle c_{21} \rangle$	5.85	1723(46)	73(2)
$\langle c_{31} \rangle$	5.85	1149(15)	49.2(8)
$\langle \gamma_{\text{loc}} \rangle$	5.85	0.63(1)	0.73(1)
$\langle \gamma_{\text{loc}} \rangle$	5.7	0.56(2)	0.76(5)
$\langle \gamma_{\text{loc}} \rangle$	5.6	—	0.53(3)

Table 1: *The characteristic indicators for the kernel condition number and for the locality of the overlap operators D_N (standard) and D_{ovHF} (described in the text), on a $12^3 \times 24$ lattice.*

Following the usual convention we take here the distance in the taxi driver metrics $\|y\|_1 := \sum_{\mu} |y_{\mu}|$. A comparison, still at $\beta = 5.85$, is given in Fig. 2 (on top) and Table 1; we see a clear gain for D_{ovHF} , i.e. a decay of $f(r_1) \propto \exp(-\gamma_{\text{loc}} r_1)$ (beyond short r_1) where γ_{loc} is larger for D_{ovHF} than for D_N . If we refer to the Euclidean distance $r = |y|$, the maximum is taken over different sets, but the resulting decay is still exponential. In the lower plot of Fig. 2 we see that the decay for D_{ovHF} is not only faster, but it also follows in a smoother way the exponential shape in r , which hints at a good approximation to rotation symmetry.

Locality is a vital requirement for a safe continuum limit in lattice field theory [26]. This poses a limitation on the overlap operator (2.6), since for decreasing β , at some point an exponential decay is not visible any longer.⁴

Fig. 3 shows the situation at $\beta = 5.7$ (i.e. $a \simeq 0.17$ fm), where both operators are still local (with optimal parameters μ and u for D_N resp. D_{ovHF}), but again the locality of D_{ovHF} is superior. As we push further to $\beta = 5.6$, we do not observe an exponential decay for D_N anymore, but D_{ovHF} is still manifestly local (even without adjusting the parameters in eq. (2.5), except for u). Therefore, the overlap-HF provides *chiral fermions on coarser lattices*.

3 Applications in the p -regime

To handle strong interactions at low energy, χ PT replaces QCD by an effective Lagrangian. It involves the terms allowed by the symmetries,

⁴The question, in which sense locality still persists in a conceptual sense is discussed in Ref. [33]. In any case, if no exponential decay is clearly visible, the operator should certainly not be applied in simulations.

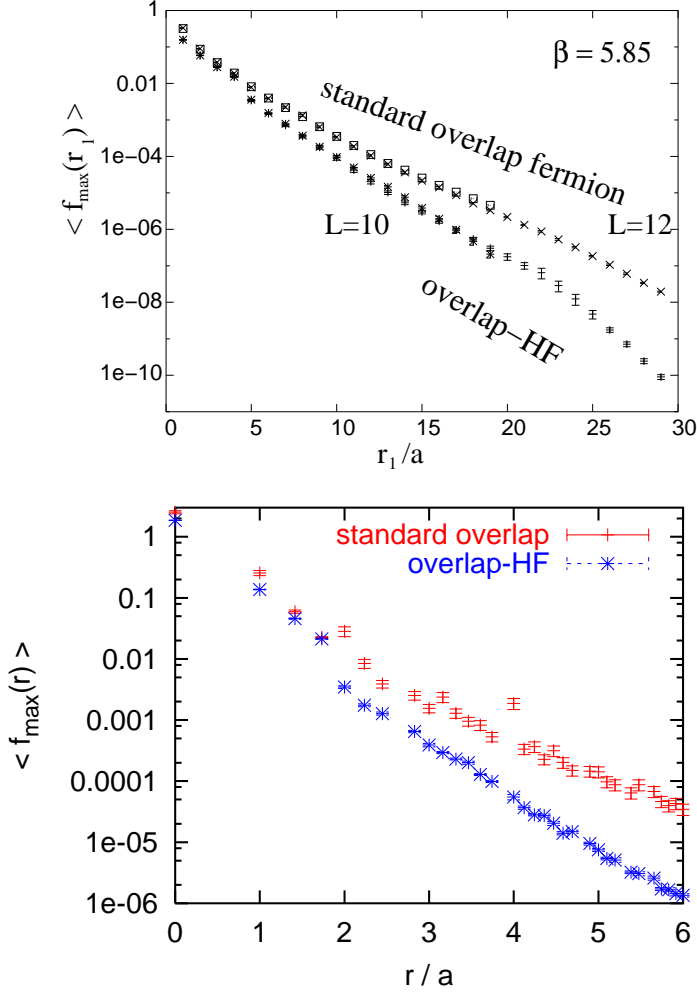


Figure 2: The locality of different overlap fermions, measured by the maximal impact of a unit source η_x over a taxi driver distance r_1 (on top), and over a Euclidean distance r (below), at $\beta = 5.85$. We see that the overlap-HF is clearly more local. The upper plot also shows that the slope hardly changes if we proceed from a 10^4 to a $12^3 \times 24$ lattice. (The increasing slope beyond $r_1 = 18$ is a consequence of the anisotropy of the $12^3 \times 24$ lattice.) The lower plot illustrates additionally that the overlap-HF decay follows closely an exponential in the Euclidean distance, which indicates a good approximation to rotation symmetry.

which are ordered according to a low energy hierarchy. To its leading order, the effective Lagrangian of χ PT takes the form

$$\mathcal{L}_{\text{eff}}[U] = \frac{F_\pi^2}{4} \text{Tr} \left[\partial_\mu U(x)^\dagger \partial_\mu U(x) \right] - \frac{\sum m_q}{2} \text{Tr} \left[U(x) + U(x)^\dagger \right] + \dots \quad (3.1)$$

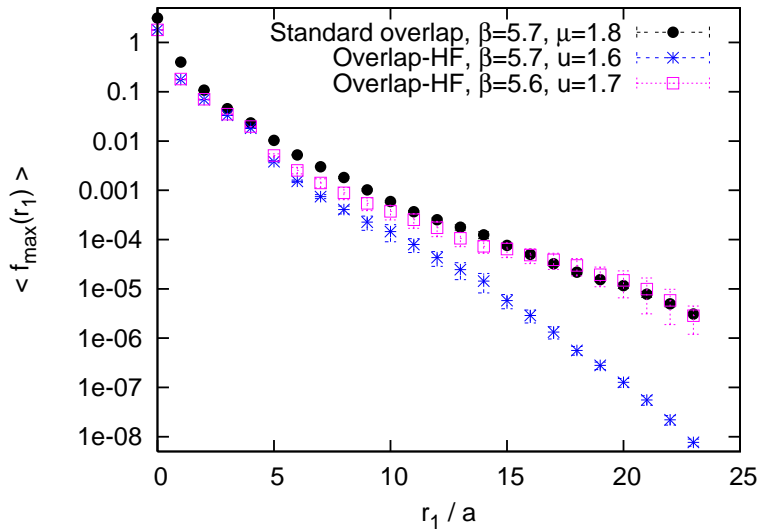


Figure 3: *The locality of different overlap fermions, measured by the maximal impact of a unit source η_x over a taxi driver distance r_1 , on a $12^3 \times 24$ lattice. For the overlap-HF we see a superior locality at $\beta = 5.7$. Its locality persists up to $\beta = 5.6$, where no exponential decay is visible for the standard overlap formulation.*

Throughout this work, we assume a degenerate quark mass m_q for all flavours involved. The LECs are the coefficients attached to the terms in this expansion; in the leading order F_π and Σ . The effective theory does have its predictive power, but the values of the LECs cannot be determined within χ PT. To this end, one has to return to QCD as the fundamental theory, and it is our main goal in this work to investigate how far the LECs can be obtained from lattice QCD simulations.

In χ PT, one usually considers a finite spatial box, which has a volume L^3 , and one expects the meson momenta p to be small, so that

$$p \sim \frac{2\pi}{L} \ll 4\pi F_\pi. \quad (3.2)$$

Note that the term $4\pi F_\pi$ takes a rôle analogous to Λ_{QCD} .

χ PT then deals with a perturbative scheme for the momenta and masses of the light mesons, with appropriate counting rules. The most wide-spread variant of χ PT assumes the volume to be large, $L \gg \xi = 1/m_\pi$ (where ξ is the correlation length, given by the inverse pion mass). Then the *p-expansion* [4] can be applied. This is an expansion in the following dimensionless ratios, which are expected to be small and counted in the same order,

$$\frac{1}{LF_\pi} \sim \frac{p}{\lambda_{\text{QCD}}} \sim \frac{m_\pi}{\lambda_{\text{QCD}}}. \quad (3.3)$$

In this Section we present our simulation results in the p -regime. We apply the overlap-HF described in Section 2, at $\beta = 5.85$ on a lattice of size $12^3 \times 24$, which corresponds to a physical volume of $V \simeq (1.48 \text{ fm})^3 \times 2.96 \text{ fm}$. We evaluated 100 propagators for each of the bare quark masses

$$am_q = 0.01, 0.02, 0.04, 0.06, 0.08 \quad \text{and} \quad 0.1$$

(in physical units: 16.1 MeV . . . 161 MeV), using a Multiple Mass Solver. We will see that the smallest mass in this set is at the edge of the p -regime — even smaller quark masses will be considered in Section 4.

We include m_q in the overlap operator (2.6) in the usual way,

$$D_{\text{ov}}(m_q) = \left(1 - \frac{am_q}{2\mu}\right) D_{\text{ov}} + m_q, \quad (3.4)$$

which leaves the largest real overlap Dirac eigenvalue invariant. m_q represents the bare mass for the quark flavours u and d .

We first evaluate the pion mass in three different ways:

- $m_{\pi,PP}$ is obtained from the decay of the pseudoscalar correlation function $\langle P(x)P(0) \rangle$, with $P(x) = \bar{\psi}_x \gamma_5 \psi_x$. This is the most obvious method, but it is not the best one in this case, as we will see.
- $m_{\pi,AA}$ is extracted from the decay of the axial-vector correlation function $\langle A_4(x)A_4(0) \rangle$, with $A_4(x) = \bar{\psi}_x \gamma_5 \gamma_4 \psi_x$.
- $m_{\pi,PP-SS}$ is obtained from the decay of the difference $\langle P(x)P(0) - S(x)S(0) \rangle$, where $S(x) = \bar{\psi}_x \psi_x$ is the scalar density. This subtraction is useful especially at small m_q , where configurations with zero-modes ought to be strongly suppressed by the fermion determinant. In our quenched study, this suppression does not occur as it should, but the above subtraction in the observable eliminates the zero-mode contributions, which are mostly unphysical.

We present the results in Fig. 4 and Table 2 (the latter collects all the results of this Section). The pion masses follow to a good approximation the expected behaviour $m_\pi^2 \propto m_q$. Deviations show up at the smallest masses, where we observe the hierarchy

$$m_{\pi,PP} > m_{\pi,AA} > m_{\pi,PP-SS}, \quad (3.5)$$

in agreement with Ref. [10]. This shows that the scalar density subtraction is in fact profitable, since it suppresses the distortion of the linear behaviour down to the lightest pion mass in Fig. 4,

$$m_{\pi,PP-SS}(am_q = 0.01) = (289 \pm 32) \text{ MeV}. \quad (3.6)$$

That mass corresponds to a ratio $L/\xi \approx 2$, hence around this point we are indeed leaving the p -regime. Based on the moderate quark masses in Fig. 4, we find an impressively small intercept in the chiral extrapolation,

$$m_{\pi,PP-SS}(m_q \rightarrow 0) = (-2 \pm 24) \text{ MeV} . \quad (3.7)$$

On the other hand, at our larger m_q values the hierarchy changes due to the interference of the scalar correlator.

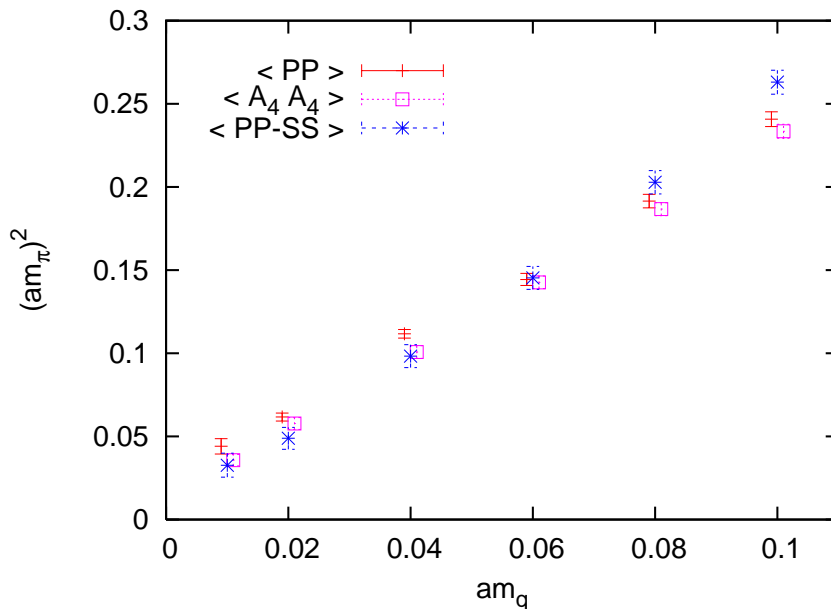


Figure 4: *The pion mass evaluated from overlap HFs in the p -regime in three different ways, as described in Section 3.*

Due to quenching, one expects at small quark masses a logarithmic behaviour of the form

$$\frac{am_\pi^2}{m_q} = C_1 + C_2 \ln am_q + C_3 am_q , \quad (C_1, C_2, C_3 : \text{constants}) . \quad (3.8)$$

Corresponding results are given for instance in Refs. [34, 35]. Fig. 3.8 shows the fits of our data to eq. (3.8). $m_{\pi,AA}$ is best compatible with this rule (this property was also hinted at in Ref. [35]). At least the deviation for $m_{\pi,PP-SS}$ (although inside the errors) could be expected, since the scalar subtraction alleviates the quenching artifacts, which give rise to the logarithmic corrections according to formula (3.8).

In Fig. 6 (and Table 2) we consider the vector meson mass m_ρ based on the same 100 configurations. A chiral extrapolation leads to

$$m_\rho = (1017 \pm 40) \text{ MeV} . \quad (3.9)$$

am_q	0.1	0.08	0.06	0.04	0.02	0.01
$am_{\pi,PP}$	0.491(5)	0.438(5)	0.380(5)	0.314(4)	0.248(5)	0.210(11)
$am_{\pi,AA}$	0.483(4)	0.432(5)	0.378(5)	0.317(6)	0.240(7)	0.189(9)
$am_{\pi,PP-SS}$	0.513(7)	0.453(8)	0.381(9)	0.313(11)	0.221(15)	0.181(20)
am_ρ	0.745(7)	0.717(8)	0.694(10)	0.677(15)	0.674(32)	0.672(55)
am_{PCAC}	0.089(3)	0.070(3)	0.052(3)	0.035(3)	0.017(2)	0.0087(13)
Z_A	1.13(4)	1.14(5)	1.15(6)	1.16(9)	1.16(14)	1.14(18)
$aF_{\pi,PP}$	0.117(2)	0.114(3)	0.110(3)	0.105(4)	0.103(4)	0.098(4)
$aF_{\pi,PP-SS}$	0.120(2)	0.114(3)	0.109(3)	0.104(5)	0.010(10)	0.082(12)

Table 2: Our results in the p -regime for the pion mass, the ρ -meson mass, the PCAC quark mass, the renormalisation constant Z_A and the pion decay constant F_π , as described in the text and plotted in the Figures of Section 3 (Figs. 4 . . . 9). These results are obtained from 100 propagators at each of the bare quark masses m_q . All the dimensional numbers in this Table are given in lattice units at $a \simeq 0.123 \text{ fm} = (1610 \text{ MeV})^{-1}$.

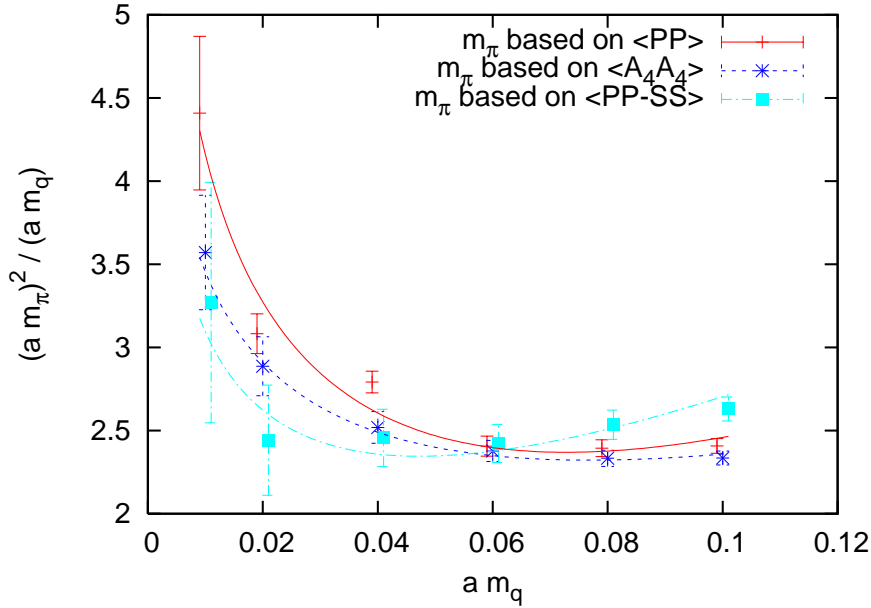


Figure 5: The pion masses of Fig. 4, fitted against the form (3.8), which is expected for the logarithmic quenching artifacts in the absence of an additive mass renormalisation.

This agrees well with a study using the standard overlap operator on the same lattice [36]. It is quite large, however, not only in view of phenomenology, but also compared to other quenched results in the lit-

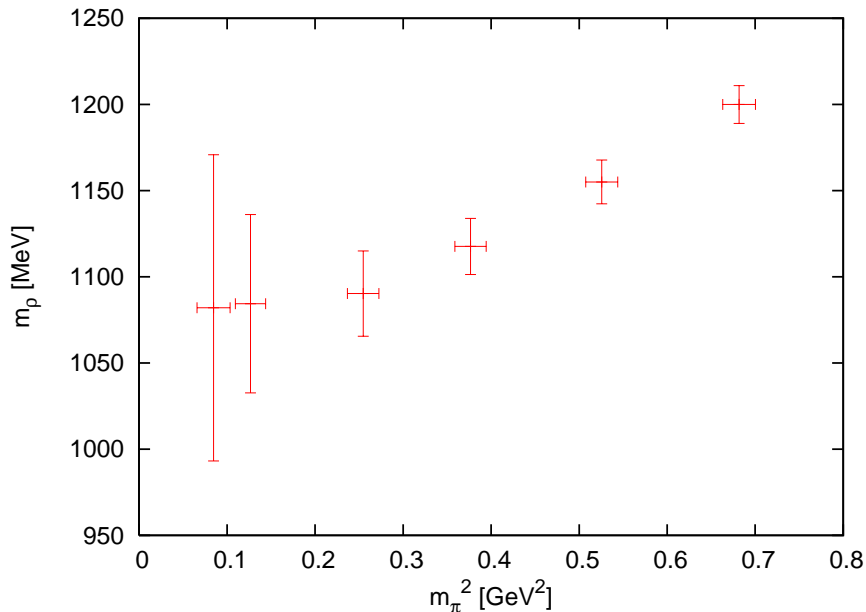


Figure 6: *The mass of the ρ -meson against the squared pion mass $m_{\pi,PP-SS}^2$.*

erature, which were summarised in Ref. [37].⁵

On the other hand, if we insert our measured ratio $m_{\text{pseudoscalar}}/m_{\text{vector}}$ at $m_q = 0.01$ into the phenomenologically motivated interpolation formula presented in Ref. [38], then we arrive at a significantly lower value of $m_\rho \approx 789$ MeV.

Fig. 7 shows the quark mass obtained from the PCAC relation,

$$m_{\text{PCAC}} = \frac{\sum_{\vec{x}} \langle (\partial_4 A_4^\dagger(x)) P(0) \rangle}{\sum_{\vec{x}} \langle P^\dagger(x) P(0) \rangle}, \quad (3.10)$$

which follows closely the bare quark mass m_q (we use a symmetric nearest-neighbour difference for ∂_4). As a consequence, the axial-current renormalisation constant

$$Z_A = \frac{m_q}{m_{\text{PCAC}}} \quad (3.11)$$

is close to 1, see Fig. 8 and Table 2. A chiral extrapolation leads smoothly to

$$Z_A = 1.17(2), \quad (3.12)$$

which is in contrast to the unpleasantly large values found for the standard overlap operator: e.g. at the same $\beta = 5.85$ and $\mu = 1.6$ (a preferred

⁵Note that the difference from the data by other groups — obtained with various (mostly non-chiral) lattice formulations — is approximately constant in m_π over the range shown here, hence finite size effects can hardly be blamed for it.

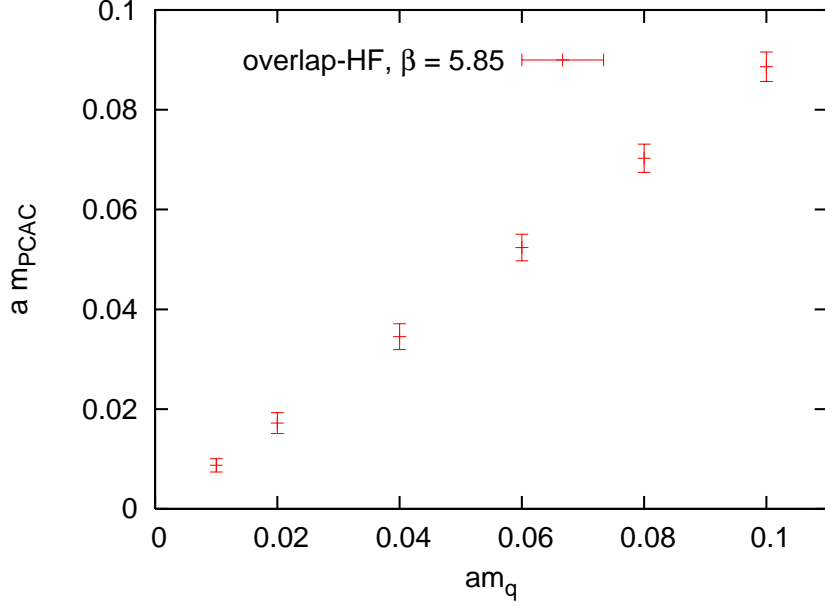


Figure 7: The PCAC quark mass, evaluated for D_{ovHF} according to eq. (3.10), from stable plateaux in the time direction. We find m_{PCAC} values close to m_q , in contrast to the results with the standard overlap operator.

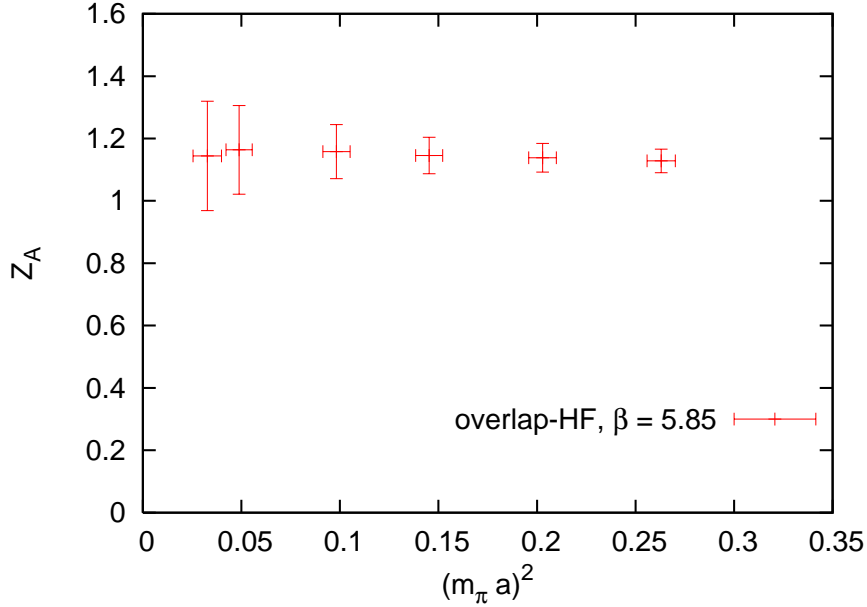


Figure 8: The axial-current renormalisation constant Z_A , determined from eq. (3.11), which is found to be close to 1 for the overlap-HF. Z_A is plotted against $m_{\pi,PP-SS}^2$.

value in that case) it amounts to $Z_A \simeq 1.45$ [36, 39, 40], and (somewhat surprisingly) at $\beta = 6$, $\mu = 1.4$ it even rises to $Z_A \simeq 1.55$ [40]. According to Ref. [32], the fat link could be especially helpful for the property $Z_A \approx 1$, which is favourable for a connection to perturbation theory.

As a last observable in the p -regime, we measured the pion decay constant by means of the (indirect) relation

$$F_\pi = \frac{2m_q}{m_\pi^2} |\langle 0|P|\pi\rangle| , \quad (3.13)$$

based on $P(x)P(0)$, or based on $P(x)P(0) - S(x)S(0)$ (in eq. (3.13) this affects both, the denominator and the pion state).⁶ The results are given in Fig. 9 and Table 2. In particular the value at $am_q = 0.01$ (the lightest quark mass in this plot) is significantly lower for the case of the scalar subtraction. Hence this pushes the result towards the chirally extrapolated phenomenological value of ≈ 86 MeV [42].

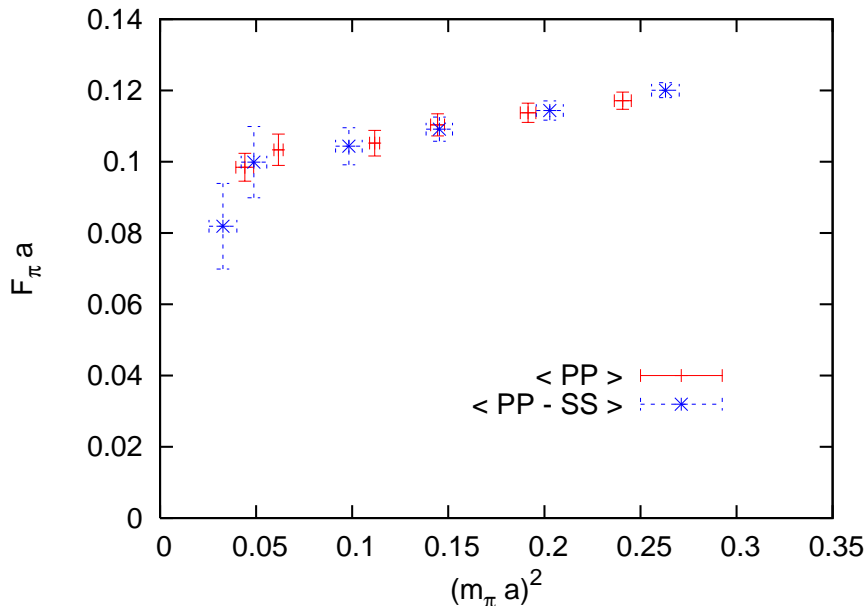


Figure 9: *The pion decay constant based on a matrix element evaluation in the p -regime — given by eq. (3.13) — using the overlap-HF.*

However, a chiral extrapolation based on these data for F_π would be risky — apparently we are too far from the chiral limit for this purpose. An extrapolated value of $F_{\pi,PP}$ would come out clearly too large, as it is also the case for D_N [36]. But in particular the instability of $F_{\pi,PP-SS}$

⁶A recent alternative attempt to evaluate LECs from simulations in the p -regime was presented in Ref. [41].

at $am_q = 0.04, 0.02, 0.01$ calls for a clarification by yet smaller quark masses. We did consider still much smaller values of m_q in the same volume. As the results for the pion masses suggest, we are thus leaving the p -regime. For the tiny masses $am_q \leq 0.005$ we enter in fact the ϵ -regime, where observables like F_π have to be evaluated in a completely different manner. This is the subject of Section 4.

4 Applications in the ϵ -regime

The ϵ -regime of QCD is characterised by a relatively small volume, i.e. the correlation length ξ exceeds the linear box size L . On the other hand, the box still has to be large compared to the scale given by $4\pi F_\pi$, as in eq. (3.2), so that the partition function is saturated by the lowest states only — higher states (above about 1 GeV) do not contribute significantly. This amounts to the condition

$$\frac{1}{m_\pi} > L \gg \frac{1}{4\pi F_\pi} . \quad (4.1)$$

In such a box, the p -expansion of χ PT fails, in particular due to the dominant rôle of the zero-modes. However, the latter can be treated separately by means of collective variables, and the higher modes — along with the pion mass — are then captured by the ϵ -*expansion* [5]. One now counts the ratios

$$\frac{m_\pi}{\Lambda_{\text{QCD}}} \sim \frac{p^2}{\Lambda_{\text{QCD}}^2} \sim \frac{1}{(LF_\pi)^2} \quad (4.2)$$

as small quantities in the same order.

The Haar measure for the fields $U(x) \in SU(N_f)$ in the coset space of the chiral symmetry breaking,

$$SU(N_f)_L \otimes SU(N_f)_R \rightarrow SU(N_f)_{L+R} \quad (\text{for } N_f \text{ flavours}) , \quad (4.3)$$

is worked out in Ref. [43]. The corresponding non-linear $O(N)$ σ -model (with a symmetry breaking to $O(N-1)$) in a small box was studied with the Faddeev-Popov method to two loops [44], and with the Polyakov functional measure to three loops [45].

This setting cannot be considered a physical situation. Nevertheless there is a strong motivation for its numerical study: the point is that the finite size effects are parametrised by the LECs of the effective chiral Lagrangian as they occur in infinite volume, hence the physical values of the LECs can (in principle) be evaluated even in an unphysically small box.

We recall that the effective chiral Lagrangian includes all terms which are compatible with the symmetries, ordered according to suitable low energy counting rules, in this case the counting rules (4.2) of the ϵ -expansion. We further presented in Section 3 the LECs as coefficients of these terms, for instance F_π and Σ in the leading order. Their determination from QCD — the fundamental theory — at low energy is a challenge for lattice simulations. As a test, such a lattice determination in the ϵ -regime has been performed successfully for the $O(4)$ σ -model (which describes chiral symmetry breaking with two flavours) some years ago [46], but in QCD this method [47] had to await the advent of chiral lattice fermions. Unfortunately, the quenched results for the LECs are affected by (mostly logarithmic) finite size effects [48], so that the final results by this method still have to wait for the feasibility of QCD simulations with dynamical, chiral quarks.

A peculiarity of the ϵ -regime is that the topological sector plays an essential rôle [49]: if one measures observables in a specific sector, the expectation values often depend significantly on the (absolute value of the) topological charge in this sector. In particular for the evaluation of the LECs, a numerical measurement inside a specific sector and a confrontation with the analytical predictions in this sector is in principle sufficient. This requires the collection of a large number of configurations in a specific sector. The “topology conserving gauge actions” [50] are designed to facilitate this task. However, here we stay with the Wilson gauge action, which allows us to investigate also the statistical distribution of the topological charges, which we are going to address next.

4.1 The distribution of topological charges

A priori, it is not obvious how to introduce topological sectors in the set of lattice gauge configurations. However, if one deals with Ginsparg-Wilson fermions, a sound definition is given by adapting the Atiyah-Singer Theorem from the continuum and defining the topological charge by the fermionic index ν [18],

$$\text{topological charge} \stackrel{!}{=} \nu := n_+ - n_- , \quad (4.4)$$

where n_\pm is the number of zero-modes with positive/negative chirality. We remark that these numbers are unambiguously determined once a Ginsparg-Wilson Dirac operator is fixed (and that in practice only chirality positive or chirality negative zero-modes occur in one configuration ⁷). However, for a given gauge configuration, the index for different

⁷This property even holds in cases where “cooling” deforms the configuration into a form, where a semi-classical picture suggests the presence of topological objects

Ginsparg-Wilson operators does not need to agree. Albeit the level of agreement should be high for smooth configurations, i.e. it should — and it does ⁸ — increase for rising values of β .

In our study, still at $\beta = 5.85$ on a $12^3 \times 24$ lattice, we compared the charges for the overlap-HF operator described in Section 2 and for the standard overlap operator D_N at $\mu = 1.6$. As an example, the histories of about 200 indices for the same configurations are compared in Fig. 10. Of course, these two types of indices are considerably correlated, but only 41% really coincide. We obtained a mean deviation of

$$\langle |\nu_{\text{ovHF}} - \nu_N| \rangle = 0.80(2) , \quad (4.5)$$

and we observed over more than 1000 configurations a maximal index difference of $|\nu_{\text{ovHF}} - \nu_N| = 5$. Still, the similarity is of course much closer

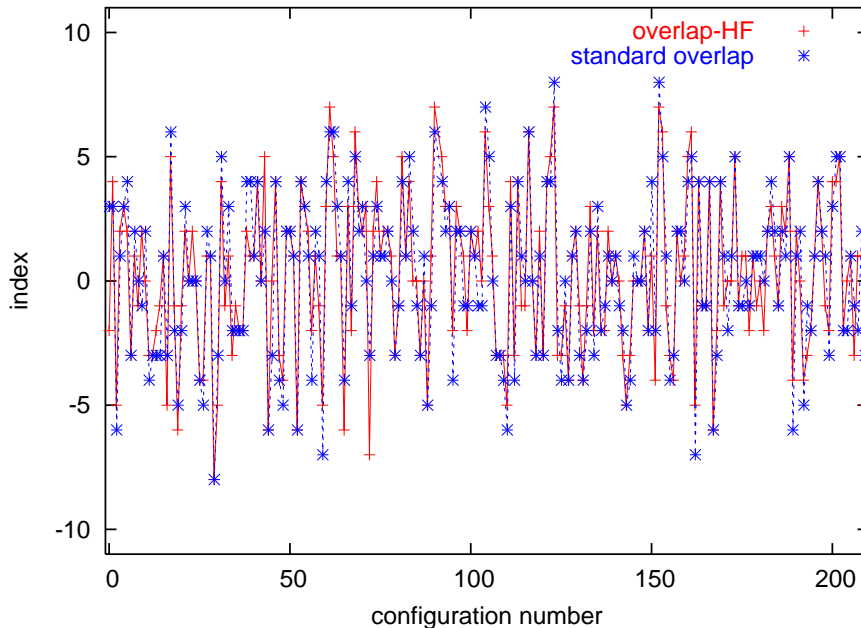


Figure 10: *Index histories for D_{ovHF} (see Section 2) and for D_N (at $\mu = 1.6$) for the same set of configurations.*

than the accidental agreement for independent indices, since they follow essentially the expected Gaussian distributions, with a width ≈ 3.3 , see Fig. 11 and Table 3. This width fixes the topological susceptibility

with opposite chiralities [51]. Regarding the fermion index, a cancellation happens for instance for free Ginsparg-Wilson fermions, but in a realistic gauge background such an unstable constellation is very unlikely.

⁸For instance, we observed at $\beta = 6.15$ on a 16^4 lattice that the index of D_N is very stable as μ rises from 1.3 to 1.7; this changes less than 2% of the indices.

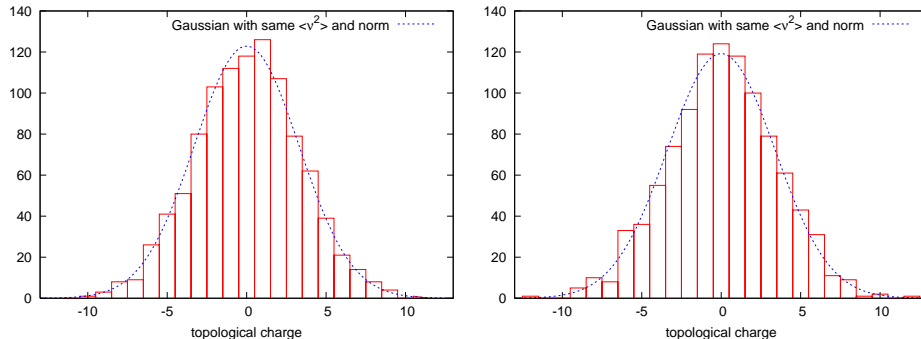


Figure 11: *The histogram of the overlap-HF indices (on the left) and for the standard overlap indices. In both cases, 1013 indices are included.*

$$\chi_{\text{top}} = \frac{1}{V} \langle \nu^2 \rangle, \quad (4.6)$$

which is of importance to explain the heavy mass of the η' meson [52]. A discussion of that point, as well as a measurement of χ_{top} based on D_N indices on L^4 lattices with a continuum extrapolation, is given in Refs. [53].

In Fig. 12 and Table 3 we present our results with D_{ovHF} and D_N on the lattice used so far, plus a result for D_N at $\beta = 6$ in the same physical volume (lattice size $16^3 \times 32$). We also mark the continuum extrapolation according to Ref. [53], which is fully consistent with our results. This value for χ_{top} is compatible with the Witten-Veneziano scenario that much of the η' mass is generated by a $U(1)$ anomaly.

In principle, the charge histogram could give insight into the possibility of a spontaneously broken parity symmetry in QCD, which is not fully ruled out [54]. This question was also studied in Ref. [55] with a different definition of topological charges on the lattice. Here we observe in all cases that the number of neutral configurations is about half of the corresponding number with $|\nu| = 1$ (see Table 3). Based on this observation, it cannot be decided if the charge distribution (at small $|\nu|$) favours a precise Gaussian, or a double peak structure (or something else). Hence the fate of parity symmetry remains open.

4.2 Determination of the chiral condensate Σ

Chiral RMT conjectures predictions for the low lying eigenvalues, ordered as λ_n , $n = 1, 2, \dots$ (excluding possible zero eigenvalues) of the Dirac operator in the ϵ -regime (for a review, see Ref. [56]). More precisely, the conjectured densities are functions of the dimensionless variables $\Sigma V \lambda_n$, where Σ is the chiral condensate in the effective Lagrangian

Dirac operator	D_{ovHF}	D_{N}	D_{N}
β	5.85	5.85	6
a	$\simeq 0.123$ fm	$\simeq 0.123$ fm	$\simeq 0.093$ fm
lattice size	$12^3 \times 24$	$12^3 \times 24$	$16^3 \times 32$
total # of confs.	1013	1013	506
$\langle \nu^2 \rangle$	10.81 ± 0.47	11.49 ± 0.51	10.49 ± 0.66
$\chi_{\text{top}} r_0^4$	0.071(3)	0.076(3)	0.069(4)
# of confs. with $\nu = 0$	118	124	59
# of confs. with $ \nu = 1$	238	237	115
# of confs. with $ \nu = 2$	210	192	95
$\Sigma^{1/3}$ from sector $\nu = 0$	298(4) MeV	301(4) MeV	279(7) MeV
$a \langle \lambda_1 \rangle_{ \nu =0}$	0.0069(4)	0.0067(4)	0.0059(4)
$a \langle \lambda_1 \rangle_{ \nu =1}$	0.0130(4)	0.0136(4)	0.0093(3)
$a \langle \lambda_1 \rangle_{ \nu =2}$	0.0184(5)	0.0193(5)	0.0130(5)
$a \langle \lambda_1 \rangle_{ \nu =3}$	0.0247(6)	0.0242(8)	0.0155(6)
$a \langle \lambda_1 \rangle_{ \nu =4}$	0.0293(9)	0.0312(10)	0.0215(9)
$a \langle \lambda_1 \rangle_{ \nu =5}$	0.0338(12)	0.0360(13)	0.0246(17)
$\Sigma^{1/3}$ from $\langle \lambda_1 \rangle_{ \nu =0\dots 5}$	290(6) MeV		

Table 3: *Our results for the topological susceptibility and for the chiral condensate in the ϵ -regime for a fixed physical volume $V = (1.48 \text{ fm})^3 \times 2.96 \text{ fm}$. We consider two types of overlap operators (D_{ovHF} as described in Section 2, and the standard overlap operator D_{N} at $\mu = 1.6$), and two lattice spacings. We first give the total statistics and the resulting topological susceptibility (see Subsection 4.1) in a dimensionless form, with $r_0 = 0.5 \text{ fm}$ (according to the Sommer scale [24]).*

Below we give separately the statistics in the sectors $|\nu| = 0, 1$ and 2. We extract the chiral condensate Σ from the density of the lowest Dirac eigenvalue in the neutral charge sector, which is most reliable since it involves the smallest values of z , see Subsection 4.2 and Figs. 13, 14.

As an alternative we considered the mean values of the lowest non-zero Dirac eigenvalues $\langle \lambda_1 \rangle$ in the sectors $|\nu| = 0 \dots 5$. For the value of Σ in the last line all these results for $\langle \lambda_1 \rangle_{|\nu|}$ match the RMT predictions, see Fig. 15.

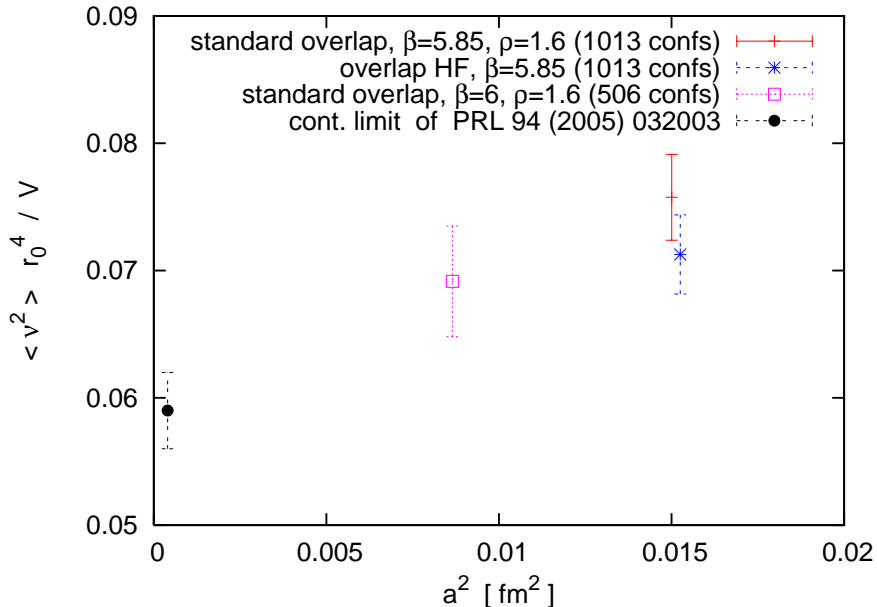


Figure 12: *The topological susceptibility measured by indices of D_{ovHF} and of D_{N} , in a volume $V = (1.48 \text{ fm})^3 \times 2.96 \text{ fm}$, with two different lattice spacings a . Our data agree well with the continuum extrapolation reported in Ref. [53].*

(3.1). Here we focus on the variable $z := \Sigma V \lambda_{1,P}$, where $\lambda_{1,P}$ emerges from the leading non-zero eigenvalue λ_1 if the spectral circle of the overlap operator is mapped stereographically on the imaginary axis, $\lambda_{1,P} = |\lambda_1 / (1 - a\lambda_1/2\mu)|$.⁹

These RMT predictions depend on $|\nu|$, the absolute value of the topological charge. Here we make use of the explicit formulae [57] for the density of the first non-zero (re-scaled) eigenvalues in the sectors $|\nu|$, which we denote by $\rho_1^{(|\nu|)}(z)$. For the lowest eigenvalues, the particular density $\rho_1^{(0)}$ was first confirmed by staggered fermion simulations (results are summarised in Ref. [56]), but the charged sectors yielded the very same density, in contradiction to RMT. The distinction between the topological sectors was first observed to hold for D_{N} to a good precision [58], if the linear box size exceeds a lower limit of about $L \gtrsim 1.1 \text{ fm}$ (of course, the exact limit depends on the criterion).¹⁰ Once the predicted density $\rho_1^{(|\nu|)}$ is well reproduced, we can read off the value of Σ , which is the only free fitting parameter for all topological sectors. It is most instructive

⁹Alternatively, one could simply consider $|\lambda_1|$, which are eigenvalues of $\gamma_5 D$, but for the small eigenvalues that we deal with the difference is not of importance.

¹⁰Meanwhile, a topological splitting was also observed to set in for staggered fermion if the link variables are strongly smeared [59].

to plot the cumulative densities [60], which we show in Figs. 13 and 14. We compare here the predictions to the eigenvalues $\lambda_{1,P}$, which we measured in various topological sectors. The statistics involved in each case is included in Table 3. This Table also displays the Σ values obtained in the sector $\nu = 0$, which we consider most reliable, since it deals with the lowest eigenvalues resp. energies. As a theoretical bound, one often refers to the Thouless energy $F_\pi^2/(\Sigma\sqrt{V})$, below which these predictions should hold. In our case, it translates into $z_{\text{Thouless}} \lesssim 1$, but the eigenvalue distributions follow the chiral RMT behaviour up to larger z values. Clearly, in this range it is the neutral sector ($\nu = 0$) which contributes in a dominant way, but Fig. 14 shows that in the case of D_N (for both values of β) the charged sectors $|\nu| = 1$ and 2 alone would favour a different Σ value. This ambiguity also occurs for smeared staggered fermions [59]. In the case of the D_{ovHF} , however, a unique Σ works well for all the three sectors $|\nu| = 0, 1, 2$, up to about $z \approx 3$, as we see from Fig. 13.

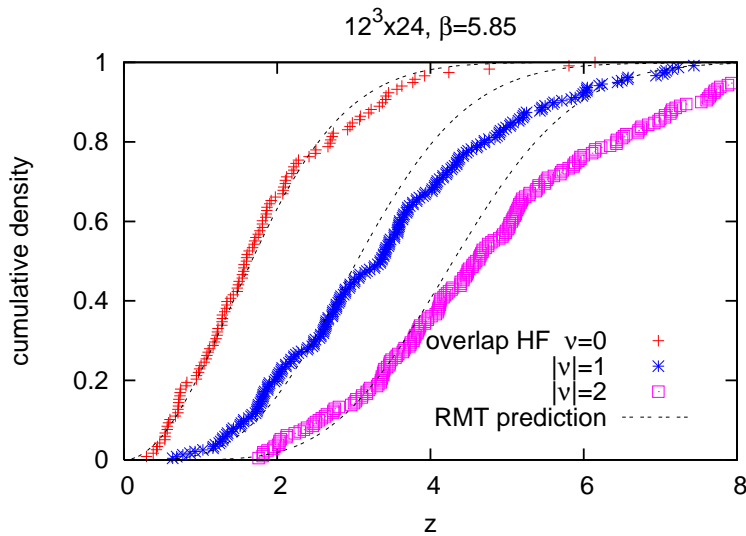


Figure 13: *The cumulative density of the lowest Dirac eigenvalue $\lambda_{1,P}$ of the overlap-HF operator, in the topological sectors $|\nu| = 0, 1$ and 2 . We compare the chiral RMT predictions to our data for $z = \Sigma V \lambda_{1,P}$ with $\Sigma^{1/3} = 298$ MeV — the optimal value in the neutral sector ($\nu = 0$). This value works well up to $z \approx 3$ for all topological sectors.*

As an alternative approach to test the agreement of our data with the chiral RMT, and to extract a value for Σ , we now focus on the mean values of the leading non-zero Dirac eigenvalues λ_1 in all the charge sectors up to $|\nu| = 5$. In physical units, the results $\langle \lambda_{1,P} \rangle$ agree remarkably well for the different overlap operators and lattice spacings — see Fig. 15 — although this consideration extends beyond very low energy. Each single

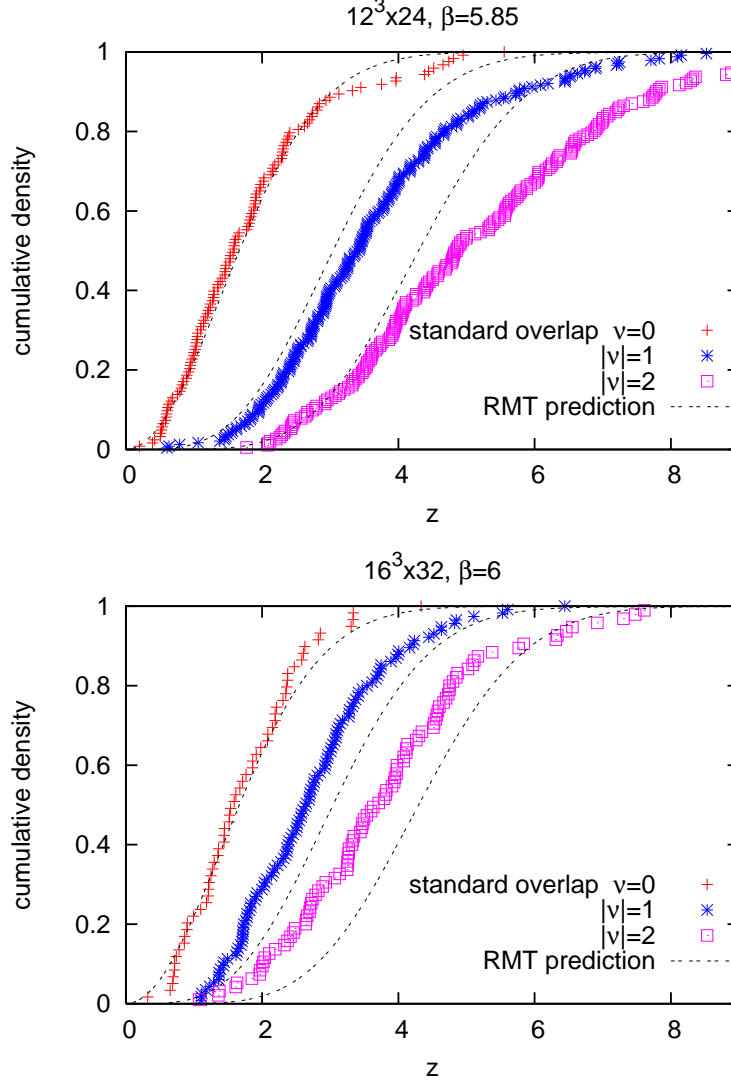


Figure 14: *The cumulative density the lowest Dirac eigenvalue $\lambda_{1,P}$ of the standard overlap operator D_N at $\beta = 5.85$ (on top) and $\beta = 6$ (below), in the topological sectors $|\nu| = 0, 1$ and 2 . We compare the chiral RMT predictions to our data for $z = \Sigma V \lambda_{1,P}$ with $\Sigma^{1/3} = 301$ MeV (on top), and with $\Sigma^{1/3} = 279$ MeV (below) — the optimal values in the neutral sector ($\nu = 0$). Considering also $|\nu| = 1, 2$ would decrease (increase) Σ at $\beta = 5.85$ ($\beta = 6$) which is the trend towards the result with the method of Fig. 15.*

result for $\langle \lambda_{1,P} \rangle_{|\nu|}$ can then be matched to the RMT value for a specific choice of Σ . Amazingly, all these 18 results are in agreement with the RMT if we fix

$$\Sigma = (290(6) \text{ MeV})^3, \quad (4.7)$$

as Fig. 15 also shows. This value is between the results obtained from the eigenvalue densities at $\nu = 0$ alone, and we recognise from Figs. 13 and 14 that this is the trend if we take the charged sectors into account.

A renormalisation procedure for Σ obtained in this way is discussed in Ref. [61]. However, we will only use this quenched lattice result as a fitting input in Section 4.3, so here we stay with the bare condensate Σ for our fixed lattice parameters.

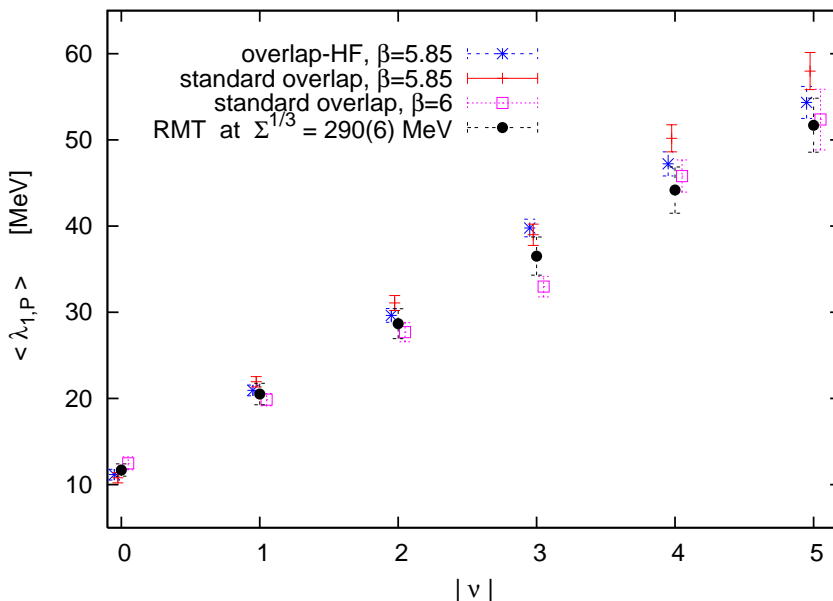


Figure 15: *The mean values of the first non-zero Dirac eigenvalue in the charge sectors $|\nu| = 0 \dots 5$, in physical unit. All the measured results agree with chiral RMT if we choose $\Sigma^{1/3} = 290(6)$ MeV.*

4.3 Evaluation of F_π based on the axial-vector current correlator

As we mentioned before, QCD simulations with chiral quarks can only be performed in the quenched approximation for the time being. In order to relate simulation results to the effective low energy theory, we therefore refer to *quenched* χPT . In that framework, mesonic correlation functions were evaluated to the first order in Refs. [62, 63]. It turned out that the vector current correlation function vanishes; this property actually extends to all orders [64]. The scalar and pseudoscalar correlators involve already in the first order additional, quenching specific LECs, which obstruct the access to the physical LECs in the Lagrangian (3.1). Therefore we first focus on the axial-vector correlator, which only depends on Σ and

F_π in the first order (as in the dynamical case). In particular we are going to compare our data to the quenched χ PT prediction in a volume $V = L^3 \times T$ [63],

$$\begin{aligned} Z_A^2 \cdot \langle A_4(t) A_4(0) \rangle_\nu &= 2 \left(\frac{F_\pi^2}{T} + 2m_q \Sigma_{|\nu|}(z_q) T h_1(\tau) \right), & (4.8) \\ h_1(\tau) &= \frac{1}{2} \left(\tau^2 - \tau + \frac{1}{6} \right), & \tau = \frac{t}{T}, \\ \Sigma_\nu(z_q) &= \Sigma \left(z_q \left[I_\nu(z_q) K_\nu(z_q) + I_{\nu+1}(z_q) K_{\nu-1}(z_q) \right] + \frac{\nu}{z_q} \right), \end{aligned}$$

where

$$A_4(t) = a^3 \sum_{\vec{x}} \bar{\psi}(t, \vec{x}) \gamma_5 \gamma_4 \psi(t, \vec{x}) \quad (t > 0) \quad (4.9)$$

is the bare axial-vector current at 3-momentum $\vec{p} = \vec{0}$. This formula applies to the topological sectors of charge $\pm\nu$. I_ν and K_ν are modified Bessel functions, and $z_q := \Sigma V m_q$ (in analogy to the variable z in Subsection 4.2).

It is remarkable that this prediction in the ϵ -regime has the shape of a *parabola* with a minimum at $t = T/2$. This is in qualitative contrast to the *cosh* behaviour, which is standard in large volumes. Σ affects both, the curvature and the minimum of this parabola, whereas F_π only occurs in the additive constant — that feature is helpful for its evaluation.

A first comparison of this curve to lattice data was presented in Ref. [65], using D_N at $\beta = 6$, $am_q = 0.01$ on lattice volumes $10^3 \times 24$ and 12^4 . The first among these volumes — with a linear size of $L \simeq 0.93$ fm — turned out to be too small: the data for $\langle A_4(t) A_4(0) \rangle_{1,2}$ were practically flat in t and incompatible with the parabola of eq. (4.8) for any positive Σ . This observation was consistent with the lower bound for L that we also found for the agreement of the microscopic spectrum with chiral RMT.

Another observation in that study was that the corresponding history in $\nu = 0$ is plagued by strong spikes, giving rise to large statistical errors. A huge statistics ($O(10^4)$ topologically neutral configurations) would be required for conclusive results (see also Ref. [66]). These spikes occur for the configurations with a tiny (non-zero) Dirac eigenvalue $\lambda_{1,P}$, and it agrees again with chiral RMT that such configurations are most frequent in the topologically neutral sector. As a remedy to this problem, a method called “low mode averaging” was designed [67].

However, without applying that method we obtained a decent agreement with the prediction (4.8) in our second volume mentioned above ($V \simeq (1.12 \text{ fm})^4$) in the sector $|\nu| = 1$, and still a reasonable shape —

although somewhat flat — at $|\nu| = 2$ [65]. In view of the leading LECs, it seems unfortunately impossible to extract a value of Σ from such data, since the theoretical curvature depends on it only in an extremely weak way (for instance, even an extreme change from $\Sigma = 0$ to $\Sigma = (250 \text{ MeV})^3$ had such a small effect that it is practically hopeless to resolve it from lattice data).¹¹

On the other hand, F_π can be extracted quite well from the vicinity of the minimum at $t = T/2$, but the value found in Ref. [65] was too high.¹²

Next a study of that kind appeared in Ref. [68], which also used D_N , at $\beta = 5.85$ and $\mu = 1.6$, now on a $10^3 \times 20$ lattice. These authors analysed the sectors $|\nu| = 0$ and 1 (without “low mode averaging”) and arrived at $F_\pi = (98.3 \pm 8.3) \text{ MeV}$. As a reason for the limitation to $|\nu| \leq 1$, Ref. [68] refers to the condition $|\nu| \ll \langle \nu^2 \rangle$. As we mentioned in Subsection 4.2, one expects $\langle \nu^2 \rangle \propto V$ (up to lattice artifacts), hence this limitation was imposed by the volume.

Here we present again results at $\beta = 5.85$ on a $12^3 \times 24$ lattice, where also the latter condition admits $|\nu| = 2$, c.f. Table 3. We evaluated for both, D_{ovHF} and D_N , the axial-vector correlators at $am_q = 0.001, 0.003$ and 0.005 , which turns out to be safely in the ϵ -regime. Our propagator statistics at these quark masses is given in Table 4. We then fitted the data to eq. (4.8) by using the chirally extrapolated factors Z_A (1.17 for D_{ovHF} and 1.45 for D_N), along with the Σ values that we obtained from the microscopic Dirac spectra (see Subsection 4.2 and Table 3). For each of the overlap operators we performed at each of the quark masses a global fit over the topological sectors that we considered, which is shown in Figs. 16 and 17. In particular our results for D_{ovHF} reveal for the first time a quite clear distinction between the sectors $|\nu| = 1$ and $|\nu| = 2$ — this property could not be observed for D_N up to now. For D_N at $am_q = 0.005$ we also include the neutral sector; as expected it has by far larger error bars than the charged sectors, but it is helpful nevertheless to reduce the error on F_π in the global fit.

The emerging values for the pion decay constant are consistent,

$$\begin{aligned} F_\pi &= (110 \pm 6) \text{ MeV} && \text{(using } D_{\text{ovHF}} \text{)}, \\ F_\pi &= (109 \pm 4) \text{ MeV} && \text{(using } D_N \text{)}. \end{aligned} \quad (4.10)$$

As an experiment, we also considered a simple re-weighting of the

¹¹Only in the sector $\nu = 0$ the sensitivity to Σ is significant, but there we run into the statistical problem mentioned before.

¹²In Ref. [65] we gave a value around 130 MeV, but the analysis did not handle the renormalisation constant Z_A very carefully — being more precise in this aspect reduces the value to about 120 MeV.

Dirac operator	D_{ovHF}	D_{N}
$am_q = 0.001$		
# of propagators at $ \nu = 1$	50	50
# of propagators at $ \nu = 2$	50	50
F_π	(110 ± 8) MeV	(109 ± 11) MeV
$am_q = 0.003$		
# of propagators at $ \nu = 1$	50	50
# of propagators at $ \nu = 2$	50	50
F_π	(113 ± 7) MeV	(110 ± 11) MeV
$am_q = 0.005$		
# of propagators at $\nu = 0$	–	100
# of propagators at $ \nu = 1$	50	100
# of propagators at $ \nu = 2$	50	100
F_π	(115 ± 6) MeV	(111 ± 4) MeV

Table 4: *Our results in the ϵ -regime for the pion decay constant F_π , based on the axial-current correlation function. The results are obtained at $\beta = 5.85$ on a $12^3 \times 24$ lattice. We give our statistics of the propagators in the different topological sectors at various bare quark masses in the ϵ -regime. (Of course, different configurations were used for D_{ovHF} and for D_{N} .) The results for F_π were determined from fits to the quenched χ PT formula (4.8) in the range $t/a \in [11, 13]$, see Figs. 16 and 17.*

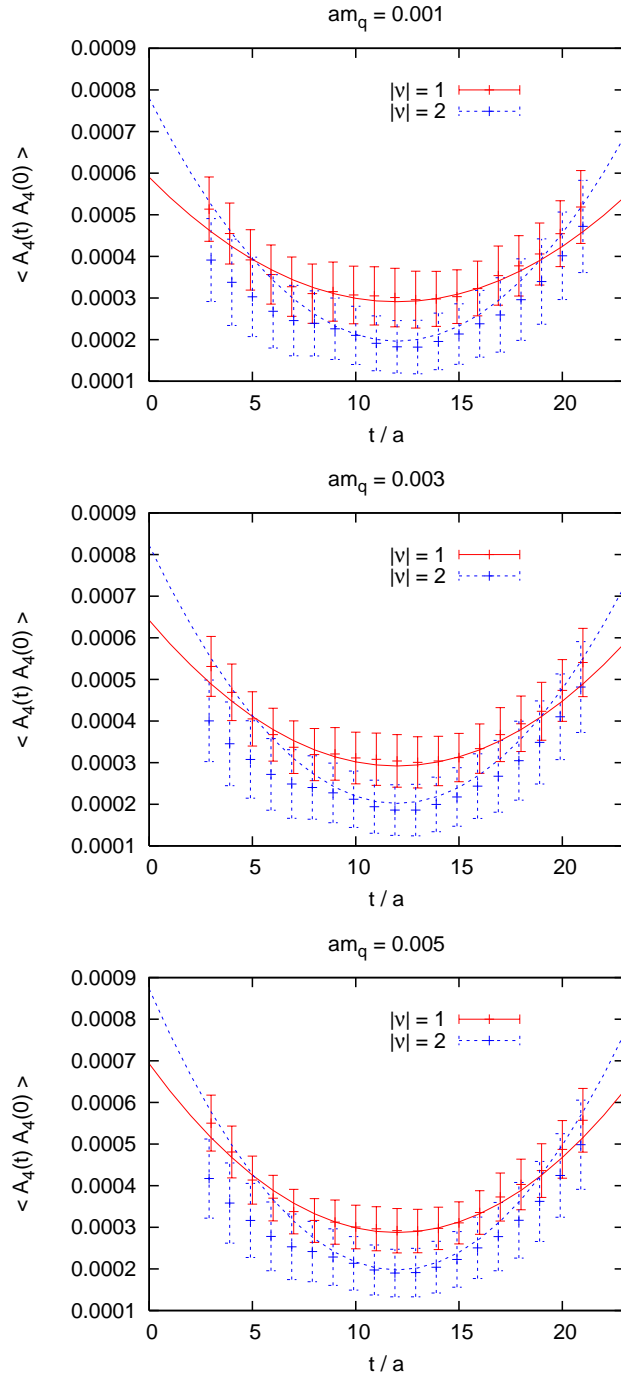


Figure 16: Lattice data with D_{ovHF} vs. predictions by quenched χ PT for the axial-current correlation functions in the ϵ -regime, measured separately in the topological sectors $|\nu| = 1$ and 2. The global fit at each mass corresponds to the values of F_π given in Table 4.

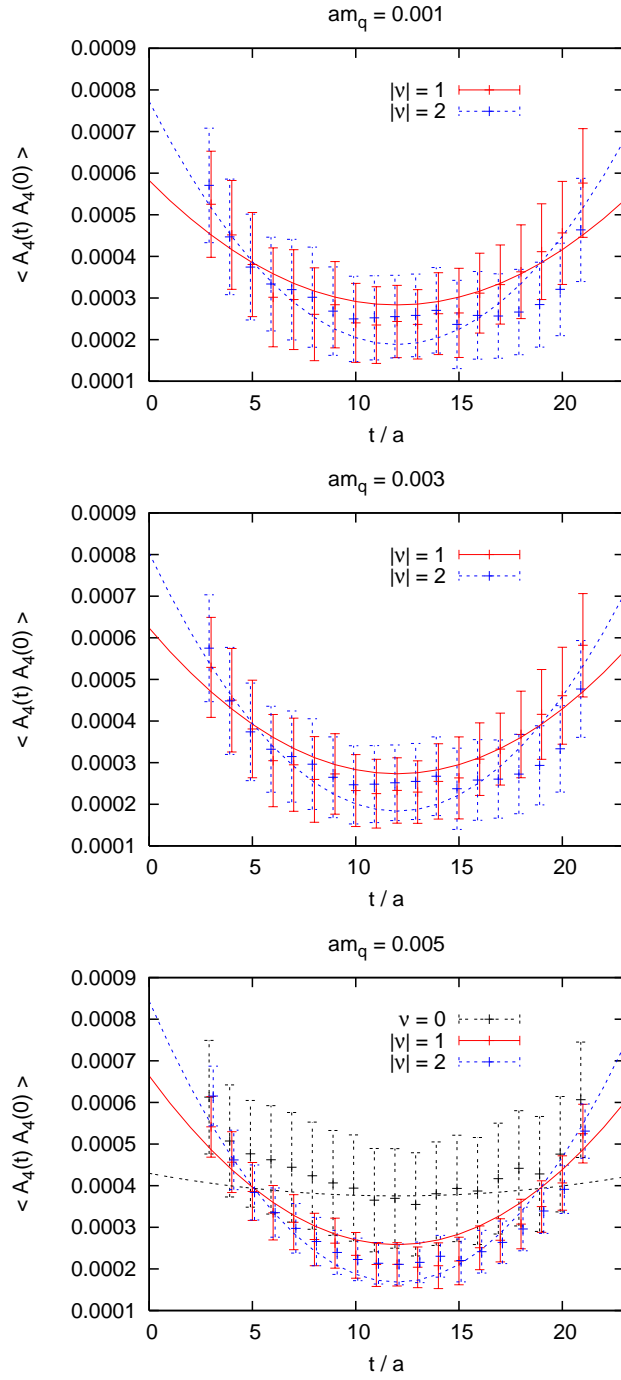


Figure 17: Lattice data with D_N vs. predictions by quenched χ PT for the axial-current correlation functions in the ϵ -regime, measured separately in the topological sectors $|\nu| = 0, 1$ and 2. The global fit at each mass corresponds to the values of F_π given in Table 4.

axial-current correlators involved, by means of the factor

$$m_q^{|\nu|} \left[m_q^2 + \left(1 - \frac{am_q}{2\mu} \right)^2 \lambda_{1,P}^2 \right], \quad (4.11)$$

which is (to a very good approximation) part of the fermion determinant. Since we take the statistics inside fixed sectors, the factor $m_q^{|\nu|}$ does not matter here, but the second factor attaches weights to the contributions, which differ in particular for very small m_q . As an example, we show in Fig. 18 the result obtained in this way for the overlap-HF at $am_q = 0.001$. Of course, this is a modest step towards a 1 flavour re-weighting, which works well in some cases if a few hundred low lying eigenvalues are involved [68, 69]. Still, in the present case we observe for the overlap-HF data an improved agreement with the predicted curves for $|\nu| = 1$ and 2 at t values relatively far from $T/2$.

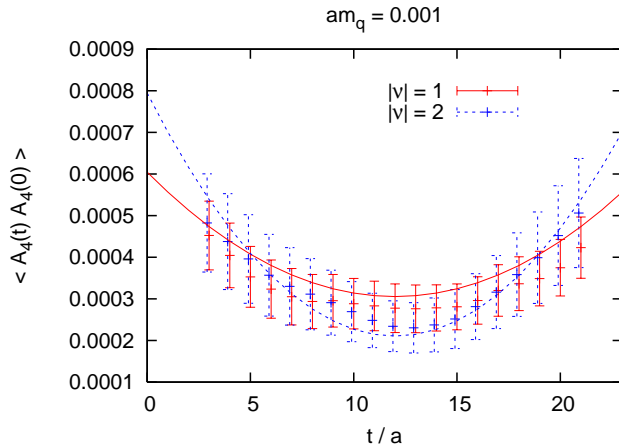


Figure 18: Lattice data with D_{ovHF} vs. predictions by quenched χ PT for the axial-current correlation functions, as in Fig. 16, but here the data are re-weighted with the first non-zero Dirac eigenvalue, i.e. with the factor (4.11). This re-weighting — which is most powerful at minimal m_q — improves the agreement with the theoretical prediction at relatively large $|t - T/2|$. In this case, the fit leads to $F_\pi = (112 \pm 7)$ MeV.

4.4 Evaluation of F_π based on the zero-modes

At last we still consider an alternative method to evaluate F_π in the ϵ -regime. This method was introduced in Ref. [70], and it involves solely the zero-mode contributions to the pseudoscalar correlation function. Hence we now work directly in the chiral limit. Let us briefly summarise the main idea of this approach.

Ref. [70] computed the chiral Lagrangian to the next-to-next-to-leading order in quenched χ PT, $\mathcal{L}_{q\chi PT}^{(2)}$. It can be written in a form that involves an auxiliary scalar field Φ_0 , which is coupled to the quasi Nambu-Goldstone field U by a new LEC denoted as K . The auxiliary field also contributes

$$\mathcal{L}^{(2)}[\Phi_0] = \frac{\alpha_0}{2N_c} \partial_\mu \Phi_0 \partial_\mu \Phi_0 + \frac{m_0^2}{2N_c} \Phi_0^2 \quad (4.12)$$

to $\mathcal{L}_{q\chi PT}^{(2)}$, which brings in α_0 and m_0 as another two quenching specific LECs, in addition to K . The inclusion of Φ_0 supplements the quenching effects; in the dynamical case it decouples from the Nambu-Goldstone field.

It is somewhat ambiguous how to count these additional terms in the quenched ϵ -expansion. Ref. [70] assumes the action terms with the coefficients α_0 and $K\sqrt{N_c}$ to be of $O(1)$, whereas the one with m_0 is in $O(\epsilon)$. In particular the last assumption is a bit unusual; for instance, it disagrees with the framework referred to in Subsection 4.3. However, it is an acceptable possibility, which simplifies this approach since it removes the auxiliary mass term from the dominant order. If one further defines the dimensionless parameter

$$\alpha = \alpha_0 - \frac{4N_c^2 K F_\pi}{\Sigma}, \quad (4.13)$$

then only the LECs F_π and α occur in this order.

For N_f valence quark flavours, we now consider the correlation function of the pseudoscalar density $P(x)$, which can be decomposed into a connected plus a disconnected part,

$$\begin{aligned} V^2 \langle P(x)P(y) \rangle &= N_f P_1(x, y) - N_f^2 P_2(x, y) \quad (4.14) \\ P_1(x, y) &= \text{Tr}[i\gamma_5(D + m_q)^{-1}(x, y) \cdot i\gamma_5(D + m_q)^{-1}(y, x)] \\ P_2(x, y) &= \text{Tr}[i\gamma_5(D + m_q)^{-1}(x, x) \cdot i\gamma_5(D + m_q)^{-1}(y, y)]. \end{aligned}$$

Then one performs a spectral decomposition of the propagators and obtains the residuum in terms of the zero-modes,

$$\begin{aligned} \lim_{m_q \rightarrow 0} (m_q V)^2 \langle P(x)P(0) \rangle_\nu &= N_f C_{|\nu|}^{(1)}(x) + N_f^2 C_{|\nu|}^{(2)}(x) \\ \text{connected : } C_{|\nu|}^{(1)}(x) &= -\langle v_j^\dagger(x) v_k(x) \cdot v_k^\dagger(0) v_j(0) \rangle_{|\nu|} \\ \text{disconnected : } C_{|\nu|}^{(2)}(x) &= \langle v_j^\dagger(x) v_j(x) \cdot v_k^\dagger(0) v_k(0) \rangle_{|\nu|}. \quad (4.15) \end{aligned}$$

The vectors v_j denote the (exact) zero-modes of the Ginsparg-Wilson operator at mass zero, $D_{\text{GW}} v_j = 0$. In the terms for $C_{|\nu|}^{(i)}$ the zero-modes are summed over.

Next we consider the spatial integral $\int d^3x P(x)P(0)$. Now the above procedure for the correlation function leads to functions $C_{|\nu|}^{(i)}(t)$, $i = 1, 2$, which are given explicitly in Ref. [70]. In principle, these functions could be measured and fitted to the predictions in order to determine F_π and α . In practice, however, it is much better to consider instead just the leading term in the expansion at $t = T/2$,

$$\frac{V}{L^2} \frac{d}{dt} C_{|\nu|}^{(i)}(t)|_{t=T/2} = D_{|\nu|}^{(i)} s + O(s^3), \quad s = t - \frac{T}{2}, \quad i = 1, 2. \quad (4.16)$$

The slopes $D_{|\nu|}^{(i)}$ tend to be stable over a variety of fitting ranges $s \in [-s_{\max}, s_{\max}]$, $s_{\max} = a, 2a, 3a \dots$. To be explicit, the slope functions [70] in a volume $V = L^3 \times T$ take the form [6]

$$D_{|\nu|}^{(1)} = \frac{2|\nu|}{(F_\pi L)^2} \left\{ |\nu| + \frac{\alpha}{2N_c} - \frac{\beta_1}{F_\pi^2 \sqrt{V}} + \left[\frac{\gamma_1}{2} - \frac{1}{24} \left(\frac{7}{3} + 2\nu^2 - 2\langle \nu^2 \rangle \right) + \frac{\gamma_1}{2} \right] \frac{T^2}{F_\pi^2 V} \right\}, \quad (4.17)$$

$$D_{|\nu|}^{(2)} = -\frac{2|\nu|}{(F_\pi L)^2} \left\{ 1 + |\nu| \left(\frac{\alpha}{2N_c} - \frac{\beta_1}{F_\pi^2 \sqrt{V}} \right) + |\nu| \left[\frac{\gamma_1}{2} - \frac{1}{24} \left(\frac{13}{3} - 2\langle \nu^2 \rangle \right) \right] \frac{T^2}{F_\pi^2 V} \right\}, \quad (4.18)$$

where in our case

$$\beta_1 = 0.1314565, \quad \gamma_1 = -\frac{1}{12} \sum_{\vec{p} \neq \vec{0}} \frac{1}{\sinh^2(T|\vec{p}|/2)} = -0.083291.$$

β_1 is a shape coefficient, which we computed for our anisotropic volume according to the prescription in Ref. [44].

We evaluated the LECs F_π and α from fits to the linear term in eq. (4.16). We used all the zero-modes that we identified in the topological sectors $|\nu| = 1$ and 2 — the statistics is given in Table 3. For $\langle \nu^2 \rangle$ (which enters the expressions for $D_{|\nu|}^{(i)}$ through Witten-Veneziano relations) we inserted the result that we measured in each case, which is also given in Table 3. For each of our lattice sizes and each type of overlap operator we performed a global fit over both topological sectors involved, in a fitting range s_{\max} . The emerging optimal values for F_π and α are shown in Figs. 19 and 20, and the values at $s_{\max}/a = 1$ are given in Table 5. We see that the results for different lattice spacings and overlap Dirac operators are in good agreement, and we obtain the most stable plateau for D_{ovHF} .

The value that we now obtain for F_π is below the one of Section 4.4, which used a different observable and a different ϵ -counting rule for the quenched terms. In fact, the result of this Section is close to the

Dirac operator	D_{ovHF}	D_N	D_N
β	5.85	5.85	6
lattice size	$12^3 \times 24$	$12^3 \times 24$	$16^3 \times 32$
F_π	(80 ± 14) MeV	(74 ± 11) MeV	(75 ± 24) MeV
α	-17 ± 10	-19 ± 8	-21 ± 15

Table 5: *Our results in the ϵ -regime for the pion decay constant F_π — along with the quenching specific LEC α — based on the zero-mode contributions to the pseudoscalar correlation function, see Subsection 4.4. The joint statistics in the sectors $|\nu| = 1$ and 2, given in Table 3, contributes. We give the results at fitting range $s_{\text{max}} = a$, which is most adequate in view of eq. (4.16).*

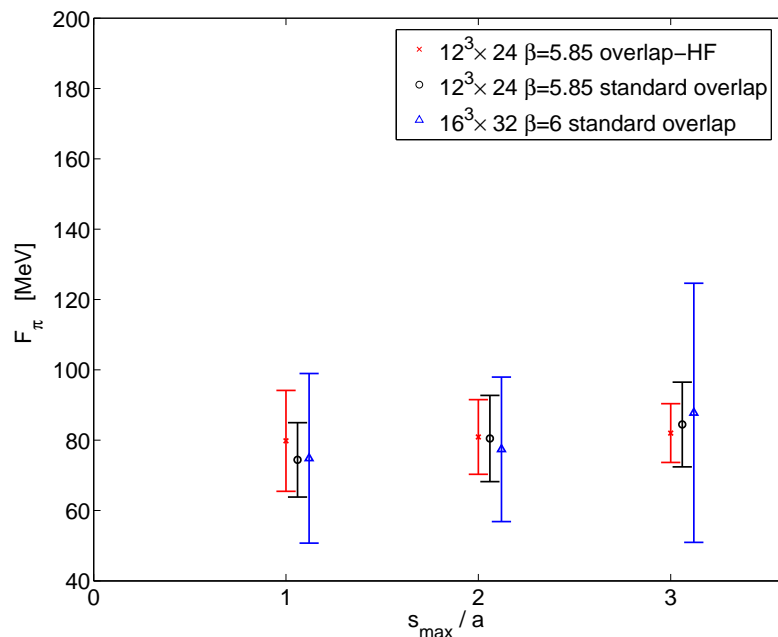


Figure 19: *The results for F_π based on a global fit of our data to a quenched χ PT prediction for the zero-mode contributions to the pseudoscalar correlations function. Here and in Fig. 20 we show the results of a two parameter fit over the ranges $s \in [T/2 - s_{\text{max}}, T/2 + s_{\text{max}}]$.*

phenomenological value (we repeat that the latter amounts to ≈ 86 MeV if one extrapolates to the chiral limit [42]). This result, as well as the negative value for α , are also somewhat below the values reported in Ref. [70] based on the same method. Some differences are that Ref. [70] always used D_N (with various values of μ), cubic volumes, a continuum extrapolated value for $\langle \nu^2 \rangle$ and partial fits were performed. We suspect

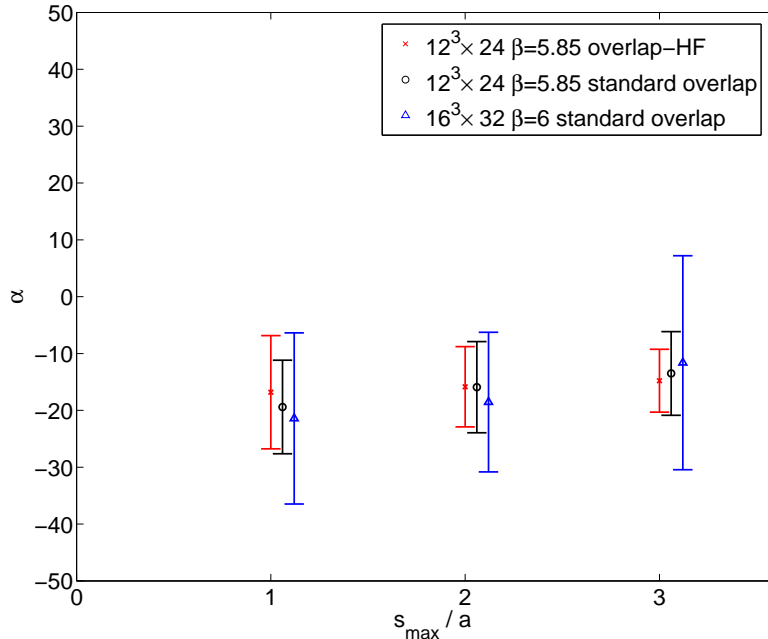


Figure 20: *The results for the quenching specific LEC α , based on a global fit of our data to a quenched χ PT prediction for the zero-mode contributions to the pseudoscalar correlations function. Here and in Fig. 19 we show the results of a two parameter fit over the ranges $s \in [T/2 - s_{\max}, T/2 + s_{\max}]$.*

that the anisotropic shape of our volumes, $T = 2L$, could be the main source of the deviation from those results [71].

5 Conclusions

We have constructed an overlap hypercube Dirac operator D_{ovHF} , which is especially suitable at a lattice spacing of $a \simeq 0.123$ fm. It has a strongly improved locality compared to the standard overlap operator D_{N} . This operator defines chiral fermions on coarser lattices than D_{N} .

We performed quenched simulations with D_{ovHF} and with D_{N} in a volume $V \simeq (1.48 \text{ fm})^3 \times (2.96 \text{ fm})$ at $\beta = 5.85$ and at $\beta = 6$.

In the p -regime we applied D_{ovHF} and measured the meson masses m_{π} and m_{ρ} , the PCAC quark mass m_{PCAC} and the pion decay constant F_{π} at bare quark masses ranging from 16.1 MeV to 161 MeV. The results for m_{π} and m_{ρ} are similar to the values found previously with D_{N} on the same lattice, which confirms their validity. On the other hand, m_{PCAC} turned out to be much closer to m_q than in the standard overlap formu-

lation. This implies an axial-current renormalisation constant close to 1, $Z_A = 1.17(2)$, which is favourable for the connection to perturbation theory. Regarding F_π , it turned out that the data obtained in the p -regime can hardly be extrapolated to the chiral limit.

We considered a large number of topological charges defined by the fermion indices of D_{ovHF} or of D_N (which coincide in part), and we found histograms which approximate well a Gaussian. The resulting topological susceptibility is in good agreement with the literature.

In the ϵ -regime we determined a value for the chiral condensate from the distribution of the lowest eigenvalues. For both, D_{ovHF} and D_N we obtained Σ values around $(300 \text{ MeV})^3$.

We evaluated F_π in the ϵ -regime in two ways, from the axial-current correlation and from the zero-mode contributions to the correlation of the pseudoscalar density. These two methods handle the ϵ -counting of the quenched terms differently, and they yield different values for F_π . The axial-current method leads to $F_\pi \approx 110 \text{ MeV}$, which is consistent with various other quenched results in the literature. The zero-mode method (which might be more sensitive to the anisotropy of the volume) leads to a lower F_π around 84 MeV , in the vicinity of the phenomenological value. The final result of Ref. [67] — using again a different method, based on the $\Delta I = 1/2$ rule, still in the ϵ -regime — is in between. We add that recently further methods were proposed to evaluate F_π in the ϵ -regime, involving $\Delta s = 1$ transitions [72] and a chemical potential [73].

From the current results, we conclude that the methods applied here work in the sense that they do have the potential to evaluate at least the leading LECs from lattice simulations in the ϵ -regime. The quenched data match the analytical predictions qualitatively (if the volume is not too small) and — in the setting we considered — they lead to results in the magnitude of the LECs in Nature. However, the quenched results are ambiguous: different methods yield different values.

For precise values and a detailed comparison to phenomenology, simulations with dynamical quarks will be needed. In particular the ϵ -regime requires then dynamical Ginsparg-Wilson fermions. For instance, quenched re-weighting already leads to a distribution of the microscopic Dirac eigenvalues and the topological charges as it is expected for one dynamical quark flavour [69]. In view of truly dynamical QCD simulations, first tests show that it is hard to arrange for topological transitions [74], but fortunately the ϵ -regime investigations can work even in a fixed topological sector. Therefore, and also in view of the lattice size, the ϵ -regime is promising, if one is able to handle sufficiently small quark

masses in a Hybrid Monte Carlo simulation, and if ergodicity inside a fixed topological sector is achieved.

Acknowledgements: *We are indebted to M. Papinutto and C. Urbach for numerical tools. We also thank A. Ali Khan, S. Dürr, H. Fukaya, P. Hasenfratz, S. Hashimoto, E. Laermann, M. Laine, K.-I. Nagai, K. Ogawa, L. Scorzato, A. Shindler, H. Stüben, P. Watson, and U. Wenger for useful comments. This work was supported by the Deutsche Forschungsgemeinschaft through SFB/TR9-03. The computations were performed on the IBM p690 clusters of the “Norddeutscher Verbund für Hoch- und Höchstleistungsrechnen” (HLRN) and at NIC, Forschungszentrum Jülich.*

References

- [1] S. Weinberg, *Physica* **A96** (1979) 327. J. Gasser and H. Leutwyler, *Ann. Phys. (N.Y.)* **158** (1984) 142.
- [2] F. Jegerlehner, *Eur. Phys. J.* **C18** (2001) 673.
- [3] S. Chandrasekharan and U.-J. Wiese, *Prog. Part. Nucl. Phys.* **53** (2004) 373.
- [4] J. Gasser and H. Leutwyler, *Phys. Lett.* **B184** (1987) 83.
- [5] J. Gasser and H. Leutwyler, *Phys. Lett.* **B188** (1987) 477. H. Neuberger, *Nucl. Phys.* **B300** (1988) 180.
- [6] S. Shcheredin, “Simulations of Lattice Fermions with Chiral Symmetry in Quantum Chromodynamics”, *Ph.D. Thesis*, Berlin (2004) [[hep-lat/0502001](#)].
- [7] W. Bietenholz and S. Shcheredin, *Rom. J. Phys.* **50** (2005) 249 [[hep-lat/0502010](#)]; *PoS(LAT2005)138* [[hep-lat/0508016](#)], *Nucl. Phys. (Proc. Suppl.)* **B153** (2006) 17. S. Shcheredin and W. Bietenholz, *PoS(LAT2005)134* [[hep-lat/0508034](#)].
- [8] K.G. Wilson and J.B. Kogut, *Phys. Rept.* **12** (1974) 75.
- [9] P. Hasenfratz and F. Niedermayer, *Nucl. Phys.* **B414** (1994) 785. T. DeGrand, A. Hasenfratz, P. Hasenfratz and F. Niedermayer, *Nucl. Phys.* **B454** (1995) 587. M. Blatter, R. Burkhalter, P. Hasenfratz and F. Niedermayer, *Phys. Rev.* **D53** (1996) 923. R. Burkhalter, *Phys. Rev.* **D54** (1996) 4121.

- [10] P. Hasenfratz, S. Hauswirth, T. Jörg, F. Niedermayer and K. Hol-
land, *Nucl. Phys.* **B643** (2002) 280. BGR Collaboration, *Nucl.*
Phys. **B677** (2004) 3.
- [11] W. Bietenholz, R. Brower, S. Chandrasekharan and U.-J. Wiese,
Phys. Lett. **B407** (1997) 283.
- [12] W. Bietenholz, E. Focht and U.-J. Wiese, *Nucl. Phys.* **B436** (1995)
385.
- [13] W. Bietenholz and U.-J. Wiese, *Nucl. Phys.* **B464** (1996) 319.
- [14] W. Bietenholz, R. Brower, S. Chandrasekharan and U.-J. Wiese,
Nucl. Phys. **B495** (1997) 285.
- [15] W. Bietenholz, R. Brower, S. Chandrasekharan and U.-J. Wiese,
Nucl. Phys. (Proc. Suppl.) **53** (1997) 921.
- [16] W. Bietenholz and U.-J. Wiese, *Phys. Lett.* **B426** (1998) 114. W.
Bietenholz, *Nucl. Phys.* **A642** (1998) 275.
- [17] P.H. Ginsparg and K.G. Wilson, *Phys. Rev.* **D25** (1982) 2649.
- [18] P. Hasenfratz, V. Laliena and F. Niedermayer, *Phys. Lett.* **B427**
(1998) 125. P. Hasenfratz, *Nucl. Phys.* **B 525** (1998) 401.
- [19] W. Bietenholz, *Eur. Phys. J.* **C6** (1999) 537.
- [20] SESAM Collaboration, *Comput. Phys. Commun.* **119** (1998) 1.
- [21] S. Wissel, E. Laermann, S. Shcheredin, S. Datta and F. Karsch,
PoS(LAT2005)164 [[hep-lat/0510031](#)].
- [22] W. Bietenholz, in Proceedings of the “International Workshop on
Non-Perturbative Methods and Lattice QCD”, Guangzhou, China
(2000) p. 3 [[hep-lat/0007017](#)].
- [23] W. Bietenholz, *Nucl. Phys.* **B644** (2002) 223.
- [24] M. Guagnelli, R. Sommer and H. Wittig, *Nucl. Phys.* **B535** (1998)
389.
- [25] H. Neuberger, *Phys. Lett.* **B417** (1998) 141; *Phys. Lett.* **B427** (1998)
353.
- [26] P. Hernández, K. Jansen and M. Lüscher, *Nucl. Phys.* **B552** (1999)
363.

- [27] M. Lüscher, *Phys. Lett.* **B428** (1998) 342.
- [28] D.H. Adams, *Annals Phys.* **296** (2002) 131.
- [29] D.H. Adams and W. Bietenholz, *Eur. Phys. J.* **C34** (2004) 245.
- [30] W. Bietenholz and I. Hip, *Nucl. Phys.* **B570** (2000) 423.
- [31] T. DeGrand, *Phys. Rev.* **D63** (2001) 034503. W. Kamleh, D.H. Adams, D.B. Leinweber and A.G. Williams, *Phys. Rev.* **D66** (2002) 014501.
- [32] S. Dürr, C. Hoelbling and U. Wenger, *JHEP* **0509** (2005) 030. S. Dürr and C. Hoelbling, *Phys. Rev.* **D72** (2005) 071501.
- [33] M. Golterman and Y. Shamir, *Phys. Rev.* **D68** (2003) 074501.
- [34] P. Hasenfratz, K.J. Juge and F. Niedermayer, *JHEP* **0412** (2004) 030.
- [35] M. Gürtler, T. Streuer, G. Schierholz, D. Galletly, R. Horsley and P. Rakow, *PoS(LAT2005)077* [hep-lat/0512027].
- [36] χ LF Collaboration, *JHEP* **0412** (2004) 044.
- [37] A. Ali Khan, hep-lat/0507031.
- [38] E. Laermann, C. DeTar, O. Kaczmarek and F. Karsch, *Nucl. Phys. (Proc. Suppl.)* **73** (1999) 447.
- [39] H. Fukaya, S. Hashimoto and K. Ogawa, *Prog. Theor. Phys.* **114** (2005) 451.
- [40] R. Babich et al., *JHEP* **0601** (2006) 086.
- [41] C. Gattringer, P. Huber and C. Lang, *Phys. Rev.* **D72** (2005) 094510.
- [42] G. Colangelo and S. Dürr, *Eur. Phys. J.* **C33** (2004) 543.
- [43] F.C. Hansen, *Nucl. Phys.* **B345** (1990) 685.
- [44] P. Hasenfratz and H. Leutwyler, *Nucl. Phys.* **B343** (1990) 241.
- [45] W. Bietenholz, *Helv. Phys. Acta* **66** (1993) 633.
- [46] A. Hasenfratz et al., *Z. Phys.* **C46** (1990) 257; *Nucl. Phys.* **B356** (1991) 332. I. Dimitrovic, P. Hasenfratz, J. Nager and F. Niedermayer, *Nucl. Phys.* **B350** (1991) 893.

- [47] L. Giusti, C. Hoelbling, M. Lüscher and H. Wittig, *Comput. Phys. Commun.* **153** (2003) 31. χ LF Collaboration, physics/0309072.
- [48] P.H. Damgaard, *Phys. Lett.* **B608** (2001) 162.
- [49] H. Leutwyler and A. Smilga, *Phys. Rev.* **D46** (1992) 5607.
- [50] M. Lüscher, *Nucl. Phys.* **B549** (1999) 295. H. Fukaya and T. Onogi, *Phys. Rev.* **D68** (2003) 074503. H. Fukaya, S. Hashimoto, T. Hirohashi, K. Ogawa and T. Onogi, *Phys. Rev.* **D73** (2006) 014503. W. Bietenholz, K. Jansen, K.-I. Nagai, S. Necco, L. Scorzato and S. Shcheredin, *JHEP* **0603** (2006) 017.
- [51] K.-I. Nagai, W. Bietenholz, T. Chiarappa, K. Jansen and S. Shcheredin, *Nucl. Phys. (Proc. Suppl.)* **B129** (2004) 516.
- [52] E. Witten, *Nucl. Phys.* **B156** (1979) 269. G. Veneziano, *Nucl. Phys.* **B159** (1979) 213.
- [53] L. Del Debbio and C. Pica, *JHEP* **0402** (2004) 003. L. Del Debbio, L. Giusti and C. Pica, *Phys. Rev. Lett.* **94** (2005) 032003.
- [54] V. Azcoiti and A. Galante, *Phys. Rev. Lett.* **83** (1999) 1518.
- [55] B. Alles, M. D’Elia and A. Di Giacomo, *Phys. Rev.* **D 71** (2005) 034503.
- [56] J.J.M. Verbaarschot and T. Wettig, *Ann. Rev. Nucl. Part. Sci.* **50** (2000) 343.
- [57] S.M. Nishigaki, P.H. Damgaard and T. Wettig, *Phys. Rev.* **D58** (1998) 087704. P.H. Damgaard and S.M. Nishigaki, *Nucl. Phys.* **B518** (1998) 495; *Phys. Rev.* **D63** (2001) 045012.
- [58] W. Bietenholz, K. Jansen and S. Shcheredin, *JHEP* **07** (2003) 033. L. Giusti, M. Lüscher, P. Weisz and H. Wittig, *JHEP* **11** (2003) 023. QCDSF-UKQCD Collaboration, *Nucl. Phys. B (Proc. Suppl.)* **129&130** (2004) 456.
- [59] E. Follana, A. Hart and C.T.H. Davies, *Phys. Rev. Lett.* **93** (2004) 241601. S. Dürr, C. Hoelbling and U. Wenger, *Phys. Rev.* **D70** (2004) 094502. Kit Yan Wong and R.M. Woloshyn, *Phys. Rev.* **D71** (2005) 094508.
- [60] W.H. Press, S.A. Teukolsky, W.T. Vetterling and B.P. Flannery, “Numerical Recipes”, Cambridge University Press, 1992.

- [61] J. Wennekens and H. Wittig, *JHEP* **0509** (2005) 059.
- [62] P.H. Damgaard, M.C. Diamantini, P. Hernández and K. Jansen, *Nucl. Phys.* **B629** (2002) 445.
- [63] P.H. Damgaard, P. Hernández, K. Jansen, M. Laine and L. Lellouch, *Nucl. Phys.* **B656** (2003) 226.
- [64] P.H. Damgaard, P. Hernández, K. Jansen, M. Laine and L. Lellouch, *Nucl. Phys. (Proc. Suppl.)* **129** (2004) 754.
- [65] W. Bietenholz, T. Chiarappa, K. Jansen, K.-I. Nagai and S. Shcheredin, *JHEP* **0402** (2004) 023.
- [66] P. Hernández, K. Jansen and L. Lellouch, *Phys. Lett.* **B469** (1999) 198.
- [67] L. Giusti, P. Hernández, M. Laine, P. Weisz and H. Wittig, *JHEP* **0404** (2004) 013.
- [68] H. Fukaya, S. Hashimoto and K. Ogawa, *Prog. Theor. Phys.* **114** (2005) 451.
- [69] K. Ogawa and S. Hashimoto, *Prog. Theor. Phys.* **114** (2005) 609.
- [70] L. Giusti, P. Hernández, M. Laine, P. Weisz and H. Wittig, *JHEP* **0401** (2004) 003.
- [71] M. Laine, private communication.
- [72] L. Giusti, P. Hernández, M. Laine, C. Pena, J. Wennekens and H. Wittig, *PoS(LAT2005)344* [hep-lat/0510033].
- [73] P.H. Damgaard, U.M. Heller, K. Splittorff and B. Svetitsky, *Phys. Rev.* **D72** (2005) 091501. P.H. Damgaard, U.M. Heller, K. Splittorff, B. Svetitsky and D. Toublan, *Phys. Rev.* **D73** (2006) 074023. J. Bloch and T. Wettig, hep-lat/0604020.
- [74] Z. Fodor, S.D. Katz and K.K. Szabo, *JHEP* **0408** (2004) 003. N. Cundy, S. Krieg, A. Frommer, Th. Lippert and K. Schilling, *Nucl. Phys. (Proc. Suppl.)* **140** (2005) 841. T. DeGrand and S. Schaefer, *Phys. Rev.* **D71** (2005) 034507. N. Cundy, *Nucl. Phys. (Proc. Suppl.)* **B153** (2006) 54.